HYDROGEN EMBRITTLEMENT: AN INTERFACIAL PHENOMENON

by

John A. Wagner

Thesis submitted to the Graduate Faculty of the
Virginia Polytechnic Institute and State University
in partial fulfillment of the requirements
for the degree of

MASTER OF SCIENCE

in

Materials Engineering

APPROVED:

M. R. Louthan, Jr., Chairman

D. W. Dwight

W. R. Hibbard, Jr.

December, 1982

Blacksburg, Virginia

Acknowledgements

The author would like to express his sincerest gratitude to Dr. M. R. Louthan, Jr., for his contributions and suggestions throughout this undertaking. His constant faity and support in the author's abilities were very inspirational and are deeply appreciated.

The author also wishes to extend his thanks to Dr. D. W. Dwight and Dr. W. R. Hibbard for their helpful suggestions and for serving as committee members. Also, thanks are due for Dr. R. D. Sisson, Jr., and the late Dr. T. P. Floridis whose contributions were vital in the initial stages of this thesis. Financial support by the Department of Energy is also greatly appreciated.

Thanks are also in order for: Zhang Bao-qi for his conscientious help on acoustic emission monitoring, Joe Terrel for his help on stainless steel testing, David Stafford for his metallographic work, Karen Kessinger for her time and efforts spent typing this manuscript and Jeanne Warner and her help throughout the preparation of this thesis.

Finally, the author wishes to express his deepest thanks to his parents, Robert and Patricia Wagner, and his friends. Their encouragement and companionship was instrumental throughout each stage of this endeavor.

TABLE OF CONTENTS

LIST OF FIGURES

LIST OF TABLES

SECTION I

Introduction

The adverse effects of hydrogen on engineering materials has been a common problem and intensely studied since the 1950's. In the initial hydrogen embrittlement investigations, most effects resulted from acid pickling and electrolytic charging (1). Since that time, the body of knowledge about the processes involved in hydrogen embrittlement has experienced tremendous growth. With the increasing awareness of the possibility of hydrogen damage, many historically unexplainable failures have been explained on the basis of hydrogen embrittlement. Despite the intensive research in the area of hydrogen embrittlement, a unified, coherent mechanism has evaded scientists. The number of test and specimen variables which contribute directly and indirectly to hydrogen damage is probably the major obstacle which must be overcome before a unified mechanism is established.

Due to the increasing awareness that hydrogen can have deleterious effects on the properties of many engineering materials, the importantance of characterization of hydrogen effects on the mechanical behavior has been recognized. Therefore, many studies of the effects of test and specimen variables have been made. Furthermore, since the number of materials exposed to hydrogeneous environments is increasing, a wide range of materials need to be evaluated in

terms of susceptibility to hydrogen damage. The studies described in this thesis were conducted to characterize hydrogen effects on three engineering materials. It is hoped that the results generated provide a better understanding of the process of hydrogen embrittlement of engineering materials. In particular, these studies show the importance of hydrogen interaction with interfaces in the embrittlement process.

SECTION II

Literature Survey

The effects of hydrogen on metals and alloys has remained the subject of extensive study and research for several decades. Much of the research in this area has been concerned with the characterization of hydrogen effects with respect to a particular material because the nature of the hydrogen induced effect is very dependent on the material. The compatibility of a material with hydrogeneous environments has been shown to be influenced by specimen design variables and test conditions (2-7). Specimen design variables such as strength (2), microstructure or metallurgical condition (3) and surface finish are known to play important roles in determining if a particular material is susceptible to hydrogen induced effects. In addition, test variables such as strain rate (4), temperature (5), stress state (6) and specimen geometry (7) have been shown to influence hydrogen embrittlement of materials. Throughout the literature are proposals for hydrogen embrittlement mechanisms to explain some experimental observations. It is becoming increasingly obvious that the testing technique (specimen design or test variables) affects the relative support any given data set provides a particular mechanism. There are almost a dozen proposed mechanisms (8) to explain hydrogen effects on metals and the mechanisms pertinent to

the present study include:

1) Interaction of dissolved hydrogen to reduce the cohesive strength of the lattice (9).
2) Absorption of hydrogen to increase the ease of dislocation generation and motion (10).
3) Binding of hydrogen to dislocations to provide localized high hydrogen concentration causing embrittlement of the lattice (11).

Each of these mechanisms is valid with respect to a portion of the available data, but no one mechanism is compatible with the bulk of the test data. This study was conducted to characterize the effect of hydrogen on austenitic stainless steels, mild steels and 2024 aluminum. One of the goals of this study was to use the most appropriate testing technique to evaluate one of the proposed embrittlement mechanisms.

In this section, a review of hydrogen embrittlement literature pertaining to the three materials of concern is present and is divided as follows:

2.1 Hydrogen Effects on Stainless Steel
2.2 Hydrogen Effects on Mild Steel
2.3 Hydrogen Effects on Aluminum

2.1 Hydrogen Effects on Stainless Steel

Numerous investigations have studied the deleterious effects of hydrogen on the mechanical properties of austenitic

stainless steels (12-17). Most of these studies have been concerned with hydrogen effects on tensile properties and crack growth behavior. However, very few studies to date have been conducted on hydrogen effects on the impact properties of austenitic stainless steels. Furthermore, although investigators have shown the importance of strain rate in relation to hydrogen embrittlement, none have used impact versus slow bend tests to emphasize this importance.

Since the majority of investigations have studied the effect of hydrogen on the tensile behavior of stainless steel, a review of some of the pertinent studies will be presented. In general, these investigations have shown that stainless steel samples tested in or precharged with hydrogen suffer ductility or fracture stress losses (12). For example, Louthan et al. have observed significant reductions in the ductility of fourteen different austenitic stainless steels when tested in a 69 MPa hydrogen environment (13). These investigators also found that a transformation to martensite is not necessary for a stainless steel to be susceptible to hydrogen embrittlement. In most studies of this nature, the strain rate dependence of hydrogen embrittlement is very apparent. For example, in tensile tests of tritium charged 304L samples, deformation enhanced tritium release was observed (12). This result was verified by Donovan in his study of 304L by showing that the amount

of hydrogen transported per unit strain decreases with increasing strain rate (14) and is consistent with the strain rate dependence of hydrogen embrittlement. All these studies associated hydrogen redistribution during testing with hydrogen embrittlement. However in a study of the impact behavior of hydrogen charged 304L stainless steel, Hyzack observed that for hydrogen embrittlement to occur, redistribution of hydrogen is not necessary and suggests that dislocation transport of hydrogen need not occur in the hydrogen embrittlement process (15).

Thus, by decreasing the test strain rate more hydrogen is able to segregate to highly strained regions. Such an increase in the local hydrogen concentration is reflected in a change from ductile to interfacial fracture. Caskey has observed the appearance of facets on the fracture face of 304L saturated with high pressure hydrogen which were not apparent in companion uncharged samples (16). Furthermore, it has been proposed that there is a distinct transition from ductile rupture to mixed mode fracture to interfacial fracture as the hydrogen content is increased in the test sample (17).

At the present time, most investigators agree that hydrogen embrittlement of stainless steels is a reality and that the degree of hydrogen embrittlement observed is a sensitive function of the test strain rate. This study

attempts to relate strain, hydrogen content and segregation, and temperature effects in the testing of two austenitic stainless steels charged with hydrogen.

2.2. Hydrogen Effects on Mild Steel

Most studies on hydrogen embrittlement of steels have been concerned with the effect of hydrogen on high strength steels because these steels have been shown to be very susceptible to hydrogen induced effects. Recently, however, mild steels have been studied with respect to susceptibility to hydrogen embrittlement because of their availability and good strength-to-cost ratio. Several of these studies have been conducted to characterize hydrogen effects on mild steels subjected to a complex stress state which could exist in in-service conditions. Because of the increasing interest in hydrogen effects on mild steels, this study has attempted to examine some aspects of this phenomenon and a review of the literature important to this study is presented.

Investigators have shown that, in general, hydrogen alters the ductility, strength and crack growth behavior in mild steels (11,18). Furthermore, the influence of microstructural features on the degree of hydrogen embrittlement of mild steels has become increasingly apparent (19). For example, in a study conducted by co-workers at Virginia Tech

on A-106 mild steel tested in a hydrogen environment showed that hydrogen significantly lowered the fracture stress and decreased the % reduction in area (20). Specifically, there were hydrogen induced losses in the ultimate strength and as much as 30% loss of fracture strength. In addition, this study emphasized the importance of metallographic features by observing hydrogen induced cracking from large inclusion stringers. Similar hydrogen induced effects have been observed in other studies which support the findings of the above A-106 steel study. In particular, Murali et al. have seen a ductility reduction and a decrease in fracture energy in the testing of hydrogen charged mild steel (21). Also, the testing of 1090 steel has shown the existence of hydrogen induced cracking through the observation of the growth of lenticular voids in hydrogen charged studies (22). Very few studies on hydrogen enhanced cracking have used acoustic emission to quantitatively determine the nature of crack growth behavior in mild steels as affected by hydrogen.

In the present investigation, a disk rupture assembly was used in the testing of mild steels for hydrogen susceptibility. Most of the pioneering work using this apparatus was conducted by Louthan of Virginia Tech and Fidelle of France. The main advantage of using the disk rupture assembly is that it closely models an in-service conditions by developing a biaxial stress state during pressurization.

Furthermore, the degree to which a material is susceptible to hydrogen embrittlement has been shown to be intimately related to the stress state imposed (23). A secondary advantage in using the disk rupture assembly is that the system is very simple and the test samples are relatively inexpensive (24).

Since there is general agreement between investigators that hydrogen segregates to regions of maximum lattice dilation (9) and since Fidelle has shown that disk rupture testing is more sensitive to hydrogen embrittlement than many other techniques (25), it is reasonable to assume that a biaxial stress state promotes lattice dilations. Therefore, lattice dilations caused by inclusions and other microstructural features are enhanced by imposing a biaxial stress state. If this is true, it is obvious that disk rupture testing lends itself to the characterization of hydrogen induced effects on local regions of maximum lattice dilation, in particular particle matrix-interfaces and crack tips. This investigation attempted to study hydrogen effects on biaxially stressed mild steels through metallography, fractography and acoustic emission techniques.

2.3 Hydrogen Effects on Aluminum

Several authors have observed that the fatigue crack growth in aluminum is significantly increased by the presence

of moisture (26). Such an observation has been attributed to the absorption of high fugacity hydrogen generated by the reaction between moisture and aluminum. This absorbed hydrogen has been shown to lead to various forms of hydrogen embrittlement. For example, it has been observed that hydrogen can degrade the ductility of many high strength aluminum alloys (27). Furthermore, Albrecht et al. have demonstrated that along with reducing ductility, hydrogen promotes intergranular fracture in cathodically charged samples (28). Another common effect of hydrogen on aluminum is to promote blistering. Often it is believed that variation in hydrogen content is the sole cause effecting the nature of blistering in aluminum alloys (26).

Although hydrogen embrittlement of aluminum alloy has been studied extensively and takes many forms, very little work has been specifically concerned with the effect of hydrogen on the age hardening characteristics of a precipitation hardenable aluminum alloy. Studies which have been concerned with hydrogen effects on the age hardening of aluminum have done so only in relation to the overall effects on mechanical properties. For example in the testing of 7075 aluminum, it was found that the underaged tempers were most susceptible to hydrogen embrittlement (28) as measured by the change in the % reduction in area. The only study to date which has been concerned with the specifics

of hydrogen effects on a 2000 series aluminum alloy was conducted by Hardwick et al. (29). In this study, samples of 2124 Al of seven different tempers were cathodically charged before and during tensile tests. Simultaneous straining and cathodic charging resulted in significant reduction in area losses especially in the underaged tempers. These results are consistent with the study on 7075 aluminum and are explained by hydrogen effects on the precipitation product and dislocations, but no "fundamental mechanisms" for the susceptibility of 2000 series aluminum was presented.

In this study, the effect of hydrogen on the age hardening characteristics of 2024 Al was examined with the hope of confirming the susceptibility of 2000 series aluminum to hydrogen embrittlement and to gain some insight into the mechanism by which this embrittlement occurs.

SECTION III

Methods and Materials

Many apparently contradictory mechanisms have been proposed to account for the various aspects of hydrogen embrittlement of metals. These proposed mechanisms frequently use either dislocation transport of hydrogen or hydrogen segregation to pre-existing sites to develop localized, high hydrogen concentrations. The experiments described in this thesis were conducted to characterize the dual nature of hydrogen localization in an attempt to emphasize the importance of both mobile hydrogen and hydrogen segregation in determining the overall hydrogen embrittlement process. Three engineering materials were examined in this study including:

3.1 Stainless Steel

3.2 Mild Steel

3.3 Aluminum

3.1 Stainless Steel

Two types of austenitic stainless steels were studied in this investigation: 21-6-9 (Fe, .03% C, 8.8% Mn, .01% P, .4% Si, 21% Cr, 7.1% Ni) and 304L (Fe, .03% C, 2.0% Mn, .045% P, .03% Si, 20% Cr, 12% Ni). The typical microstructures of the steels are shown in Figures 1 and 2 and the room temperature mechanical properties are listed in

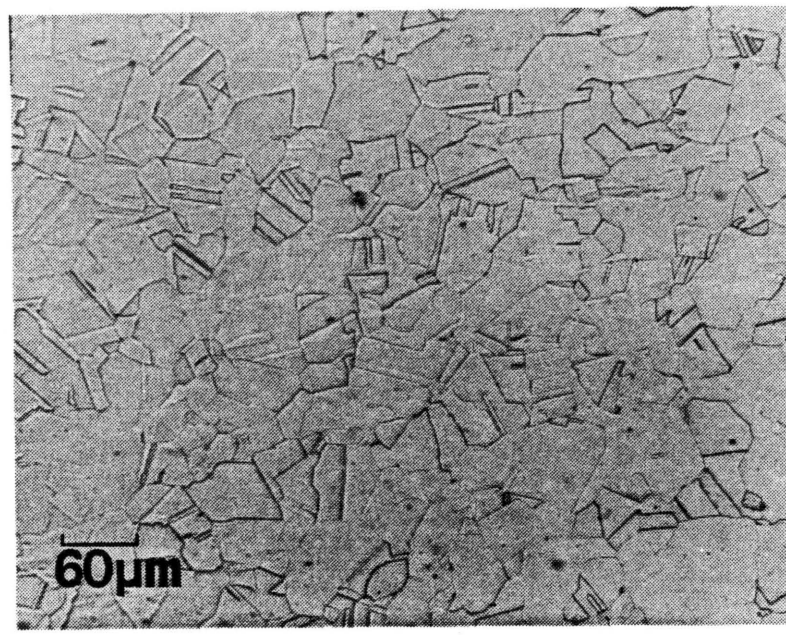

Figure 1. Microstructure of 21-6-9 stainless steel.

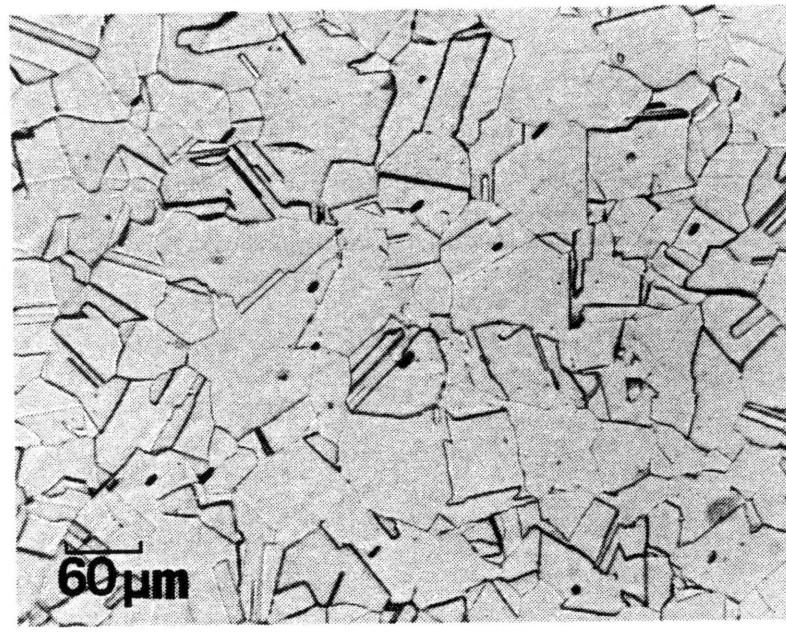

Figure 2. Microstructure of 304L stainless steel.

Table 1

Room Temperature Mechanical Properties of

21-6-9 and 304L Stainless Steels

	21-6-9	304L
Yield Strength	62.9 ksi	46.0 ksi
Ultimate Strength	112.8 ksi	88.2 ksi
% Reduction in Area	67.9	60.0

Table 1. Modified Charpy V-notch samples (ASTM E23, Type A) of annealed 304L and 21-6-9 stainless steels were machined from two inch thick cross-rolled plate stock. Samples were thermally charged with gaseous hydrogen by Sandia National Laboratory at 2,000 and 20,000 psi for 35 days at 300°C and stored at 0°C until tested.

To evaluate the extent to which hydrogen redistribution during testing is a prerequisite for hydrogen embrittlement of stainless steel, two types of tests were employed with nearly identical samples. These tests were:

3.11 Instrumented Impact Tests

3.12 Slow Bend Tests

3.11 Instrumented Impact Tests

To determine if hydrogen segregation to pre-existing sites degrades the mechanical properties of stainless steel, hydrogen charged samples were tested in an instrumented impact machine. Tests were conducted at room temperature (25°C) and liquid nitrogen temperature (-196°C). The high strain rate achieved during testing made dislocation transport of hydrogen negligible, and the low temperature of the liquid nitrogen test essentially prevented any diffusion during the very short test times. Thus, any hydrogen embrittlement effects observed in the impact tests, particularly in the tests at liquid nitrogen temperatures, can be attributed to hydrogen at pre-existing sites.

An oscilloscope read-out of the energy absorbed and the maximum load were recorded in each test. The energy absorbed was also verified by comparison with a mechanical scale. A typical oscilloscope read-out is shown in Figure 3. Fractographic studies were conducted on select samples to characterize the fracture surfaces and to determine the effect of hydrogen charging on fracture mode.

3.12 Slow Bend Tests

The role of dislocation transport in the embrittlement process for these austenitic stainless steels was determined from slow bend tests which were conducted on Charpy-V samples identical to those tested in the impact studies. The strain rate in the slow bend tests did not vary during the test process, because the cross-head motion of the deflecting ram was constant at 0.002 in/min. For each test, the distance the cross-head traveled versus the load was recorded. By integrating the area under the crosshead displacement versus load curve, the total energy absorbed for each test was obtained. These results were compared with the results of the impact tests for each material under a given charging and temperature condition, and the effect of hydrogen redistribution during test on the total energy absorbed at fracture could be established.

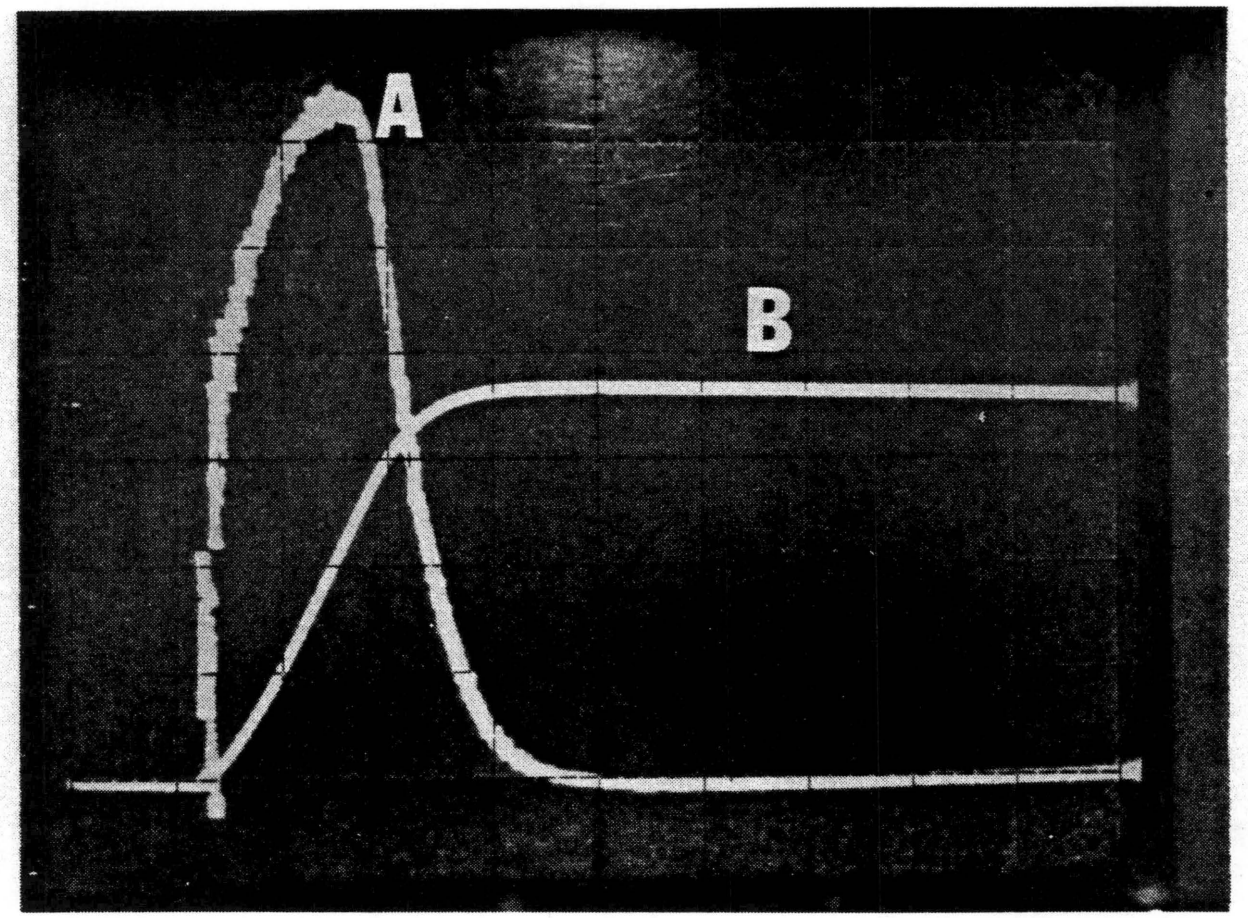

Figure 3. Typical oscilloscope read-out from instrumented impact tester. Curve A represents the load and curve B represents the energy absorbed.

3.2 Mild Steel

AISI 1015 and 1018 steels were also used to investigate the dual nature of hydrogen localization processes. The typical microstructures of the 1015 and 1018 steels are seen in Figures 4 and 5 and the room temperature mechanical properties of these alloys are summarized in Table 2. Note the relatively large inclusions in the 1018 steel. These inclusions were strung-out in the rolling direction.

The hydrogen embrittlement studies were made by conducting tests in the disk rupture assembly (Figure 6) using thin circular disks (.04 cm) machined from steel plate stock received in the spheriodized condition. Each steel disk was clamped into place with a washer of defined radius and by employing a washer with a large radius, a biaxial state of stress could be developed at the center of the sample which closely models many in-service conditions for hydrogen storage systems. In all experiments, hydrogen and oxygen were used as the test gases to pressurize one side of the disk sample and cause plastic strain and finally fracture of the specimen. To avoid contamination of the hydrogen gas, the disk rupture assembly was flushed with hydrogen and evacuated a minimum of three times prior to each hydrogen test.

The disk rupture tests conducted can be divided into two groups:

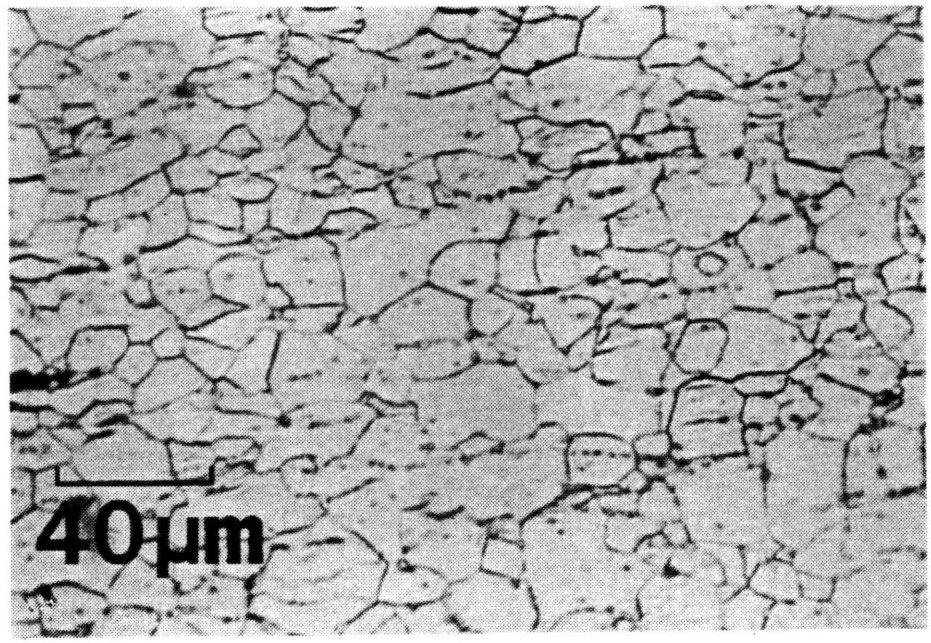

Figure 4. Microstructure of AISI 1015 steel.

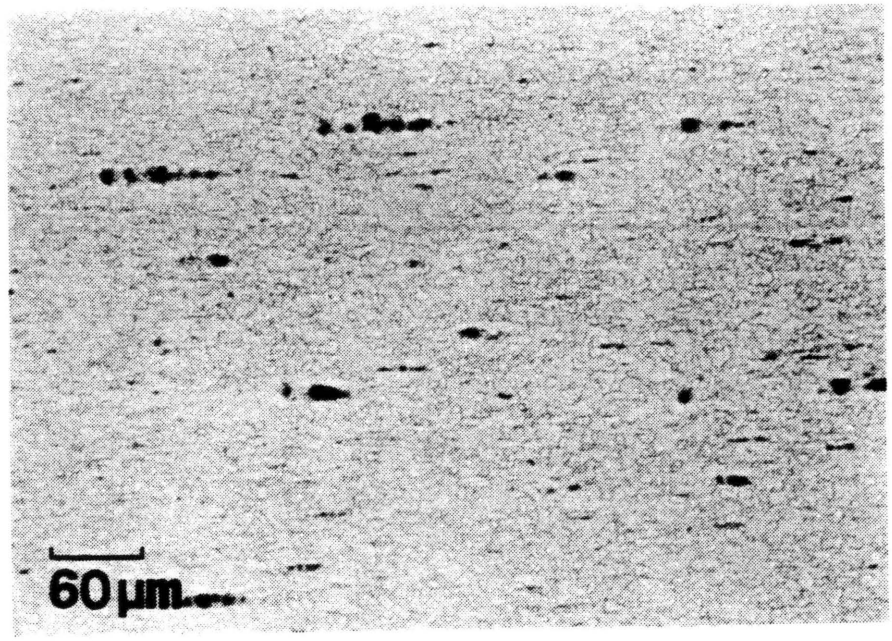

Figure 5. Microstructure of AISI 1018 steel.

Table 2

Room Temperature Mechanical Properties of

AISI 1015 and 1018 Steels

	1015	1018
Yield Strength	45.5 ksi	47.0 ksi
Ultimate Strength	61.0 ksi	63.0 ksi
% Reduction in Area	61	60

SCHEMATIC OF DISK PRESSURIZING ASSEMBLY

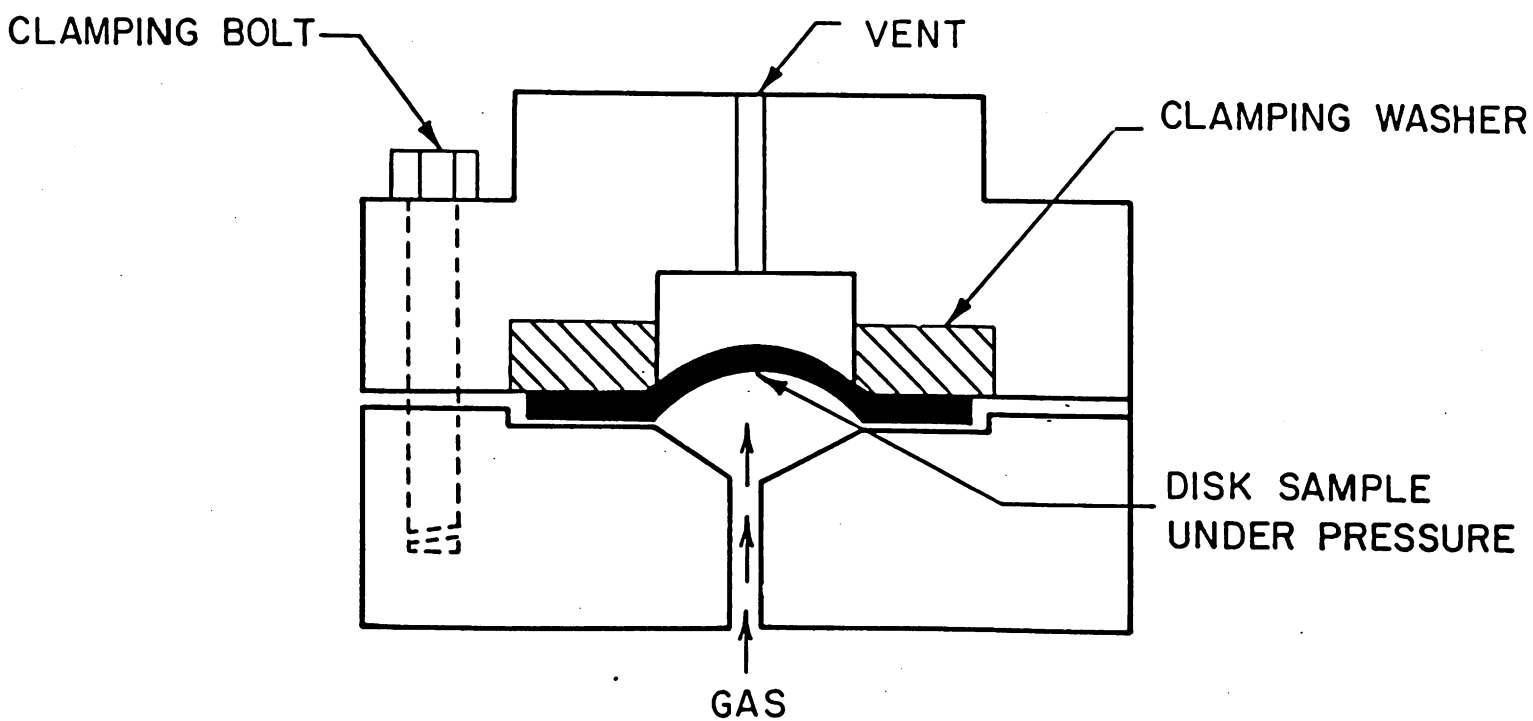

Figure 6

3.21 Simple Monotonic Pressurization Tests

3.22 Pressurization Tests with Accompanying Acoustic Emission Studies

Test gas, time to failure, failure pressure and failure mode were noted for each sample and metallographic and fractographic studies were conducted on selected specimens.

3.21 Monotonic Tests

Monotonic pressurization tests were conducted using .04 cm thick AISI Type 1018 steel disks. Prior to testing, the surface of each sample was ground and/or polished to various surface finishes (240, 320, 400, 600 grits, 1 μm and .05 μm alumina polishes). Profilometry scans of selected samples with different surface finishes were made to establish qualitative differences in the surface topography.

Tests were conducted by increasing the gas pressure at a controlled rate causing the sample to bulge and ultimately to fail in the presence of the test gas. Thus, the specimen strain rate could be controlled by the rate of pressurization. By examining these results in the light of previously conducted studies, the effect of hydrogen segregation to various metallographic features could be established.

3.22 Acoustic Emission Tests

Acoustic emission transducers, PVF_2 (Polyvinyl Fluoride), were attached to preflawed AISI Type 1015 steel disks to monitor crack growth of the disk rupture specimen. A block diagram of the instrumentation used to monitor the crack growth is shown in Figure 7.

The signals from the transducer were amplified with a bandpass filter and fed into an rms voltmeter. The D.C. voltage output from the rms voltmeter was used to drive a strip chart recorder. With this arrangement, acoustic emission signals were obtained from the microcracking which occurred during pressurization of the steel disks. Three test gases were used in this investigation: high purity hydrogen, commercial hydrogen and oxygen. Samples were tested in the as-received condition and with an artificial flaw induced by forcing a Rockwell diamond indenter into the sample surface. Three types of flaws were induced by varying the load on the indenter. The loads producing flaws were: 60, 100 and 150 kg on the Rockwell C diamond indenter oriented with the longest dimension of the indenter parallel to the rolling direction of the test sample. The majority of the tests were conducted with 60 kg flawed samples and all samples were pressurized to failure at a rate of 50 psi/min.

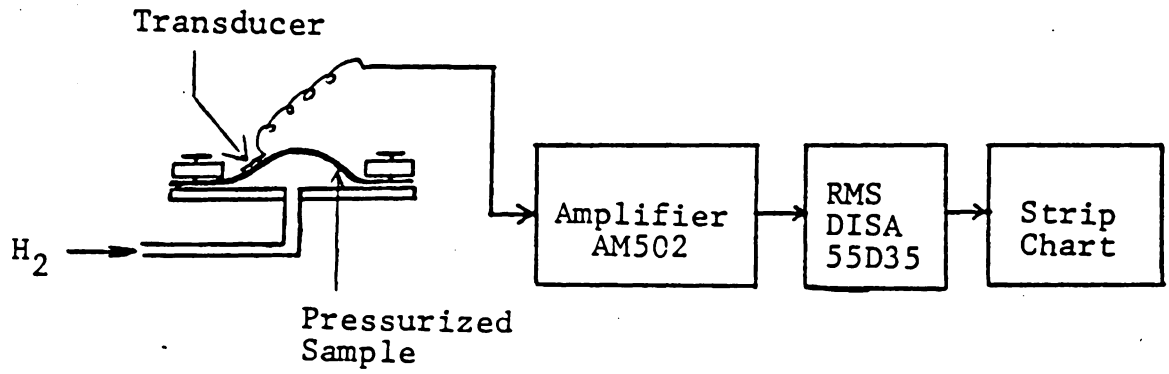

Figure 7. A block diagram of the instrumentation for Acoustic Emission Monitoring.

3.3 Aluminum

The aluminum alloy used in this study was 2024 aluminum (one of the most commonly used high strength aluminum alloys). The nominal composition of 2024 aluminum is 4.4% Cu, 1.5% Mg, 0.6% Mn balance Al and its high strength is derived from the controlled precipitation of $CuAl_2$. The microstructure and room temperature mechanical properties of the alloy are shown in Figure 8 and Table 3, respectively. This study was conducted in an attempt to determine the effect of hydrogen on the age hardening characteristics of 2024 aluminum.

Cubic samples one-half inch on edge were cut from commercial 2024 Al-T3 bar stock. The aluminum samples were exposed to a hydrogen-water vapor environment or a dry air (control) environment in two different conditions: solutionized and as-received (peak aged). The solutionized temper condition was achieved by heat treating peak aged samples at 491^{o}C for two hours. After the heat treatment, samples were water quenched and immediately stored in liquid nitrogen because 2024 aluminum will age to 90% of its peak hardness in one day at room temperature. Prior to each test, the samples were removed from the liquid nitrogen and hardness measurements were made to insure that all the samples were in the proper condition.

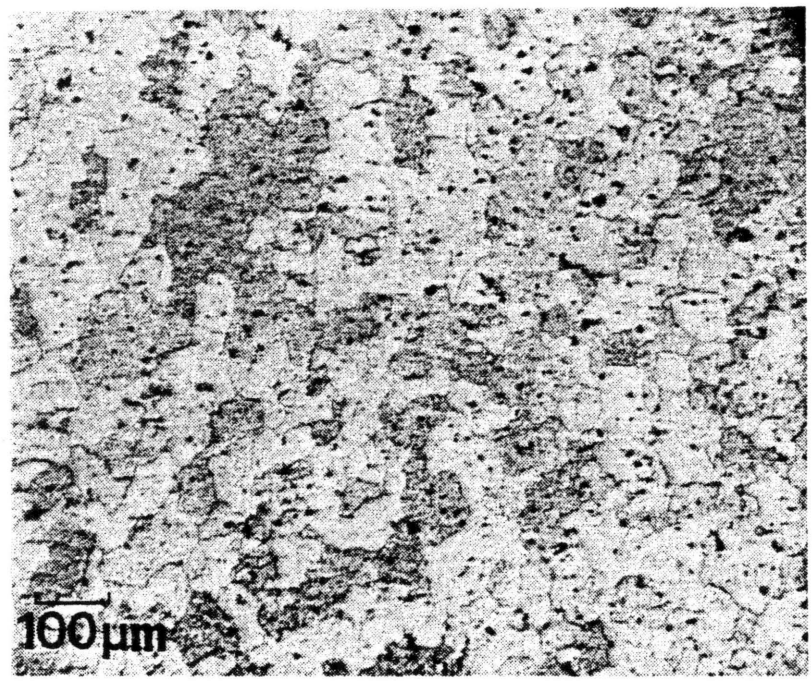

Figure 8A

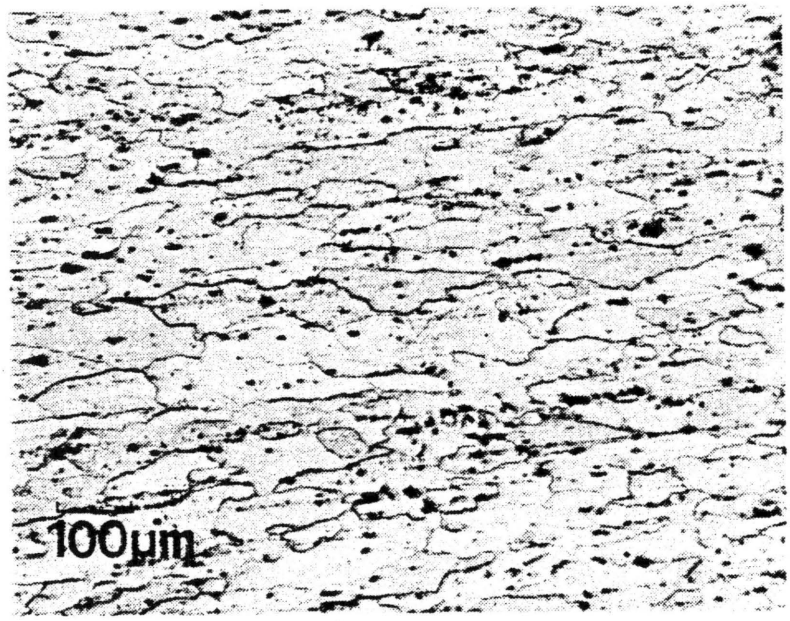

Figure 8B

Figure 8. Microstructure of 2024 aluminum: 8a) perpendicular to the rolling direction; 8b) parallel to rolling direction.

Table 3

Room Temperature Mechanical Properties

of 2024-T3 Aluminum

Yield Strength	345 MPa (50 KSI)
Ultimate Strength	485 MPa (70 KSI)
% Elongation	18%

All experiments were conducted in an apparatus which consisted of an autoclave pressure vessel surrounded by a tube furnace. Temperature control was maintained by a chromel-alumel thermocouple in combination with an Omega Digital Controller. With this experimental set-up, both temperature and pressure of the environment could be easily monitored and controlled. After initial hardness measurements were made (average of five readings), samples were loaded into a preheated autoclave and exposed to a test environment for various times. Solution treated samples were tested at 180^{o}C and exposed to either a hydrogen-water vapor environment at 1000 psi or a dry air environment. Peak aged samples were tested under the same environments, but at 240^{o}C. After exposure to an environment for a given time, samples were removed from the autoclave, quenched in water and final hardness measurements were made. By constructing hardness curves for each environment, the effect of hydrogen on the age hardening characteristics of 2024 aluminum was determined.

SECTION IV

Results and Discussion

4.1 Stainless Steel

The role of hydrogen in the embrittlement of austenitic stainless steels has been studied extensively (12-17). Although there exists a multitude of literature pertaining to effects of hydrogen on the mechanical properties of stainless steels, there is little agreement over the mechanism by which the embrittlement occurs. Much of the controversy involves the importance of test induced hydrogen redistribution in the embrittlement process. Donovan has observed significant dislocation transport of hydrogen by studying hydrogen release accompanying the plastic deformation of 304L stainless steel and proposed that this transport was a prerequisite for embrittlement (14). West and Louthan, however, demonstrated that dislocation transport of hydrogen was not required for hydrogen embrittlement during tensile tests of several austenitic stainless steels (30) and suggest that hydrogen segregation to pre-existing sites is the cause of embrittlement. Other investigators argue that dislocation transport of hydrogen is necessary for embrittlement and still other investigators propose that hydrogen at pre-existing sites causes degradation. This type of controversy has undoubtedly led to much of the disagreement which exists in the hydrogen embrittlement literature.

This study was undertaken to evaluate the separate roles of dislocation transport of hydrogen and hydrogen segregation to pre-existing sites in the overall embrittlement process. To pursue this study, impact testing (high strain rate) and slow bend testing (low strain rate) were conducted on hydrogen charged 21-6-9 and 304L stainless steel samples. By testing these samples at room temperature and liquid nitrogen temperature, the role of hydrogen at pre-existing sites and, the combined effects of hydrogen at pre-existing sites and hydrogen transported by dislocations could be differentiated and studied. This differentiation is possible since for a given charging condition any hydrogen effects exhibited in impact tests at -197^{o}C must be attributed to hydrogen at pre-existing sites and any enhancement of hydrogen effects observed in the slow bend test at 25^{o}C can be attributed to dislocation transport causing redistribution of hydrogen. The results of these tests are summarized in Table 4.

For both types of stainless steels, hydrogen charging significantly reduced both the impact and slow bend toughness at both test temperatures. The largest hydrogen effects were observed on samples tested in the slow bend mode. Also, a large difference was observed in energy absorbed in the slow bend samples and in the impact samples for any given charging and test condition. The reduction in the energy absorbed

Table 4

Energy Absorbed in Impact and Slow Bend Tests

Temperature (°C)	Charging Condition (KSI)	Energy Absorbed Impact (FT-LBS)	Energy Absorbed Slow Bend (FT-LBS)	% of Uncharged Energy* Impact	% of Uncharged Energy* Slow Bend
21-6-9 Stainless Steel					
25	0	275	145.8		
25	0	255	136.2		
25	2	235	89.4	93	64
25	2	260	91.9		
25	20	210	65.2	82	46
25	20	225	65.5		
-197	0	45			
-197	0	35	38.7		
-197	2	37	35.0	94	89
-197	2	38	33.7		
-197	20	30	21.3	69	63
-197	20	25	27.7		
304L Stainless Steel					
25	0	250			
25	0	280	144.3		
25	2	195	101.8	73	69
25	2	190	97.3		
25	20	190	75.6	75	53
25	20	205	78.1		
-197	0	260			
-197	0	185	145.7		
-197	2	170		79	99**
-197	2	180	143.9		
-197	20	160		65	39
-197	20	130	57.3		

*When there existed 2 values for a given condition, the average was used.

**Believed to be invalid (off center alignment).

for hydrogen charged samples tested in the impact mode at -197°C indicates that hydrogen redistribution during the test is not necessary for hydrogen to degrade the impact properties of stainless steel. This result is consistent with studies on Type 304L stainless steel conducted by Hyzak et al., who previously observed a reduction in impact toughness of hydrogen charged samples at -197°C (15). This effect was rationalized by noting that the diffusivity of hydrogen in austenite at -197°C is $\approx 10^{-43}$ m^2/sec and with the high strain rate of the impact test, there is a low probability for hydrogen redistribution during the test. Thus, the hydrogen induced reduction in energy absorbed was attributed to the localized high hydrogen concentration developed by thermal charging. Results of the present study confirm the importance of absorbed hydrogen in the embrittlement process and suggest that dislocation transport of hydrogen may not have a large effect on the embrittlement processes in austenitic stainless steels. This observation is contrary to the suggestions of several investigators.

However, although dislocation transport may not be playing the sole role in the hydrogen embrittlement processes of impact samples, it does contribute significantly to the overall hydrogen embrittlement process in slow bend tests. In each test conducted, slow bend samples showed a greater susceptibility to hydrogen embrittlement than the impact samples (Table 4).

Enhanced hydrogen embrittlement is reflected in the greater loss in total energy absorbed in hydrogen charged samples compared to uncharged samples. These combined observations indicate that both dislocation transport and hydrogen segregation to pre-existing sites are operative in hydrogen embrittlement processes. The enhanced embrittlement in the slow bend tests is in agreement with Donovan's observation that the amount of hydrogen transported per unit strain increases with decreases in strain rate in studies of hydrogen release during plastic deformation (14). Donovan assumes that the increase in the rate of hydrogen released is directly related to increases in the amount of dislocation transport of hydrogen.

Slow bend samples of 21-6-9 stainless steel at -197^{o}C exhibited a faceted (interfacial) type fracture (Figure 9), while impact fractures were primarily ductile rupture with some faceted features connecting the dimples (Figure 10). This result showed that strain rate affected the failure processes and that slow strain rates promoted interfacial failure. By thermally charging samples with hydrogen, the amount of interfacial fracture was increased. This tendency for interfacial fracture increases with increasing hydrogen charging pressure. Thus both hydrogen absorption and slow strain rates promoted interfacial rupture. The large well defined facets observed in hydrogen charged slow bend

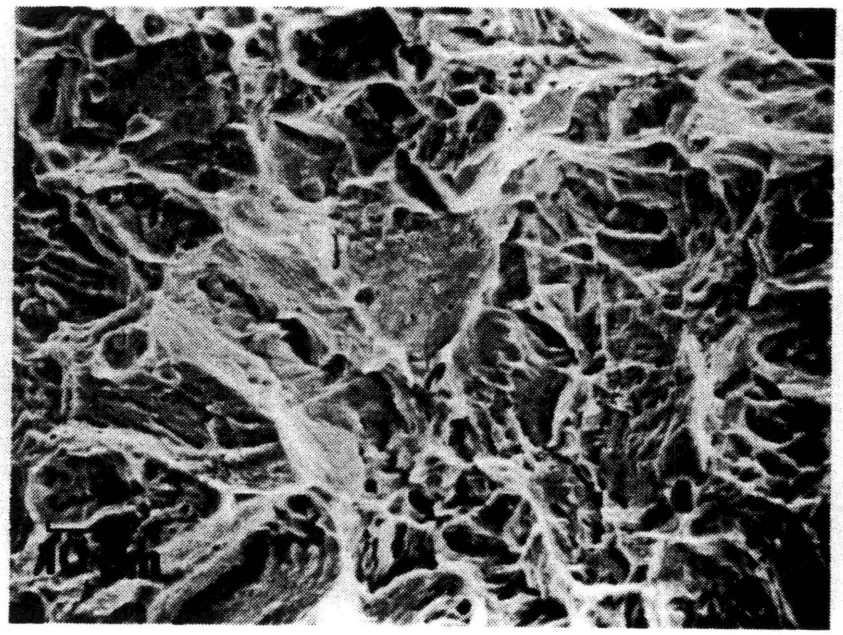

Figure 9. Fractograph of as-received 21-6-9 sample tested under slow bend conditions at -197°C.

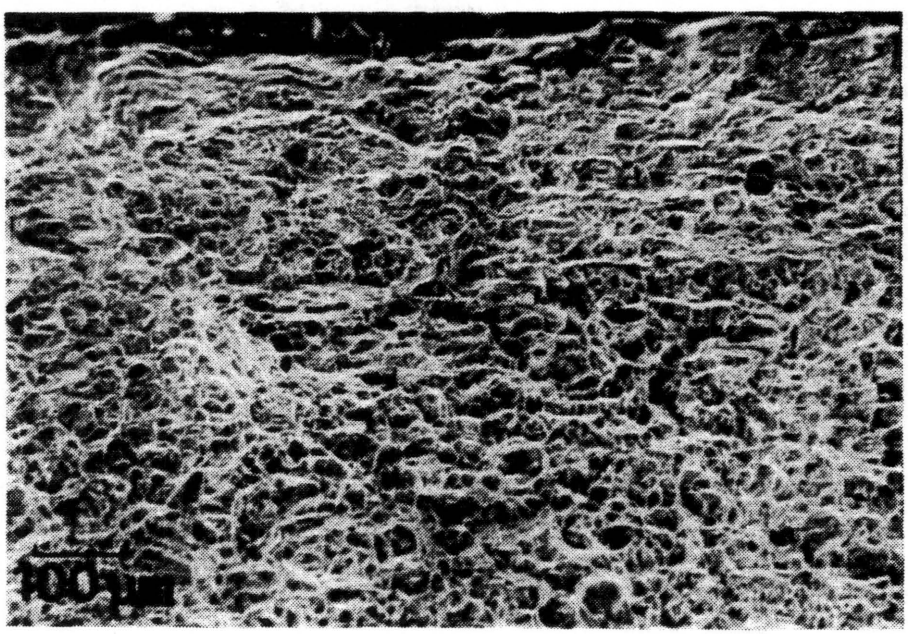

Figure 10. Fractograph of as-received 21-6-9 sample tested under impact conditions at -197°C.

samples (Figure 11) are characteristic of ductile-to-brittle transitions where the interfacial weakening represents brittle fracture. Impacted samples fractured primarily by ductile rupture processes even when charged, but there was an increase in the tendency for faceted fracture in the hydrogen charged samples (Figure 12). These results show that hydrogen absorption alone is weakening the interfaces in 21-6-9 steel but that additional hydrogen induced interfacial weakening must accompany testing and slow strain rates. All 21-6-9 impact samples tested at room temperature exhibited a dimple rupture fracture regardless of charging conditions. In slow bend tests of 21-6-9 samples, the ductile-to-brittle transition manifests itself as a fracture mode transition from dimple rupture to faceted/dimple rupture to a faceted/brittle fracture as the hydrogen charging pressures increased from 0 psi to 2,000 psi to 20,000 psi, (Figure 13).

Samples of 304L stainless steel tested at -197^{o}C fractured by dimpled rupture processes regardless of the strain rate and hydrogen charging (Figure 14), thus indicating that the interfaces were stronger relative to the matrix in 304L than in 21-6-9. All samples showing microvoid coalescence exhibit two dimple sizes and semi-quantative measurements indicate that finer dimples were associated with slow bend fractures. Impact tested samples at room

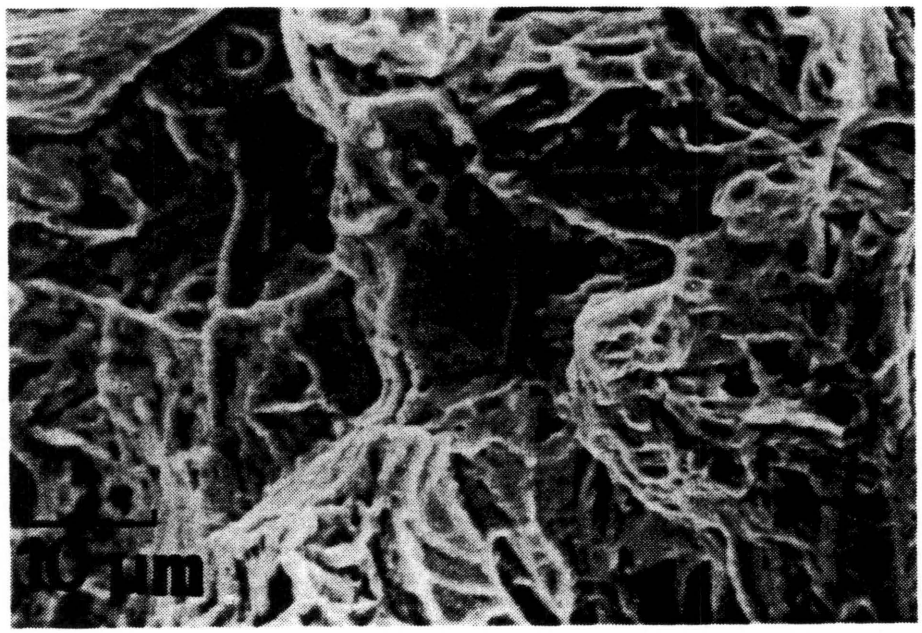

Figure 11. Fractograph of 21-6-9 sample charged with 20 ksi hydrogen and tested under slow bend conditions at -197°C.

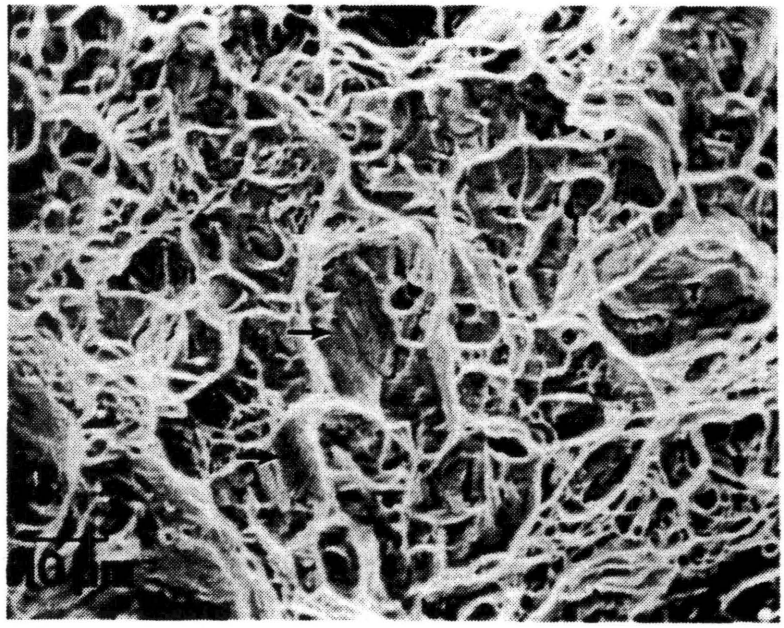

Figure 12. Fractograph of 21-6-9 sample charged with 2 ksi hydrogen and tested under impact conditions at -197°C.

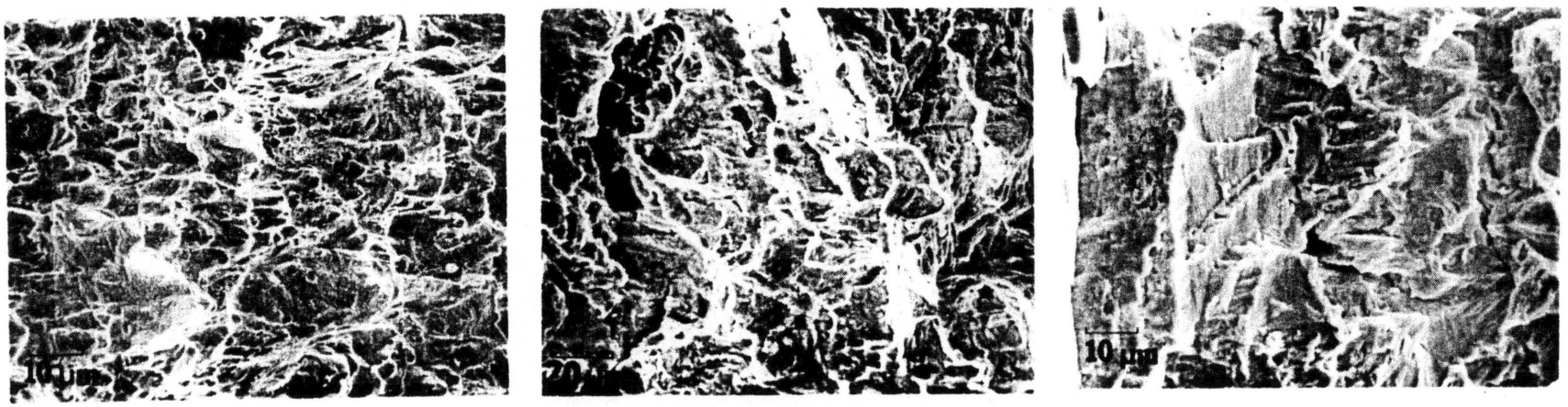

A B C

Figure 13. Fractographs of 21-6-9 samples tested at 25°C; a) uncharged, b) 2 ksi charge and c) 20 ksi charge.

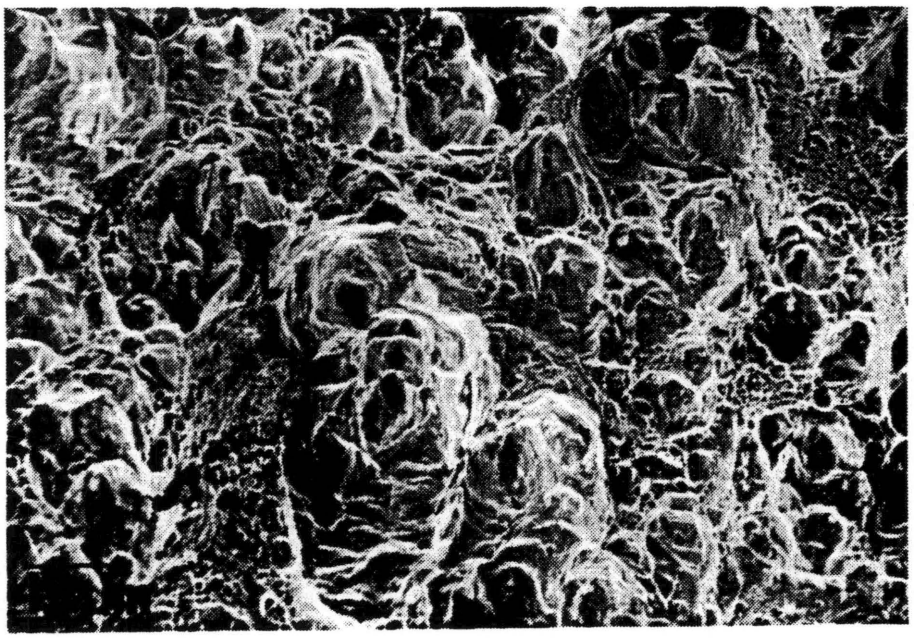

Figure 14A

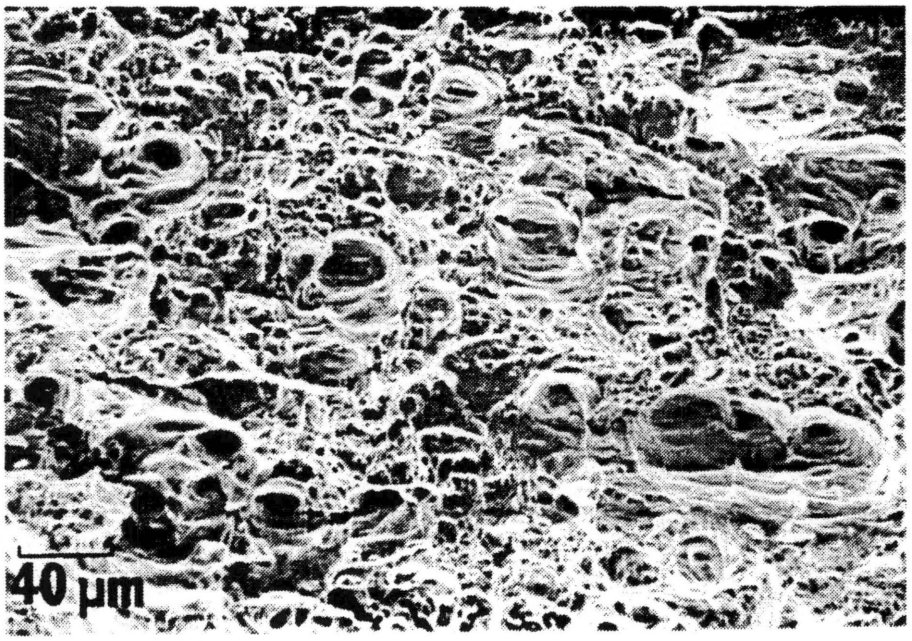

Figure 14B

Figure 14. Fractographs of 304L stainless steel samples tested at -197°C: a) impact tested, 20 ksi charged and b) slow bend tested, 2 ksi charge.

temperature also fracture by ductile rupture processes for all charging conditions and the only observable hydrogen effect was to increase the void size. Slow bend samples tested at room temperature also failed by dimple rupture, however some facets were associated with fracture in the charged samples (Figure 15).

The greater change in % of uncharged energy (Table 4) for 20 ksi hydrogen charged 21-6-9 impact samples tested at -197°C compared to those tested at 25°C is reasonable since the concentration of hydrogen at an interface, C_I, is defined by:

$$C_I = C_L \exp - \frac{GB}{RT}$$

where

C_L = concentration of hydrogen in the lattice

G_B = Binding energy of hydrogen to the interfaces (G_B is negative for segregation).

Therefore by decreasing the test temperature from 25°C to -197°C, the concentration of hydrogen at an interface increases and is reflected in a greater reduction in energy absorbed.

Hydrogen effects similar to those found in this study on austenitic steels have been discussed by several investigators, many of whom assume that hydrogen effects on austenitic stainless steels are associated with phase transformations to α' or ε martensite (31). Other investigators assume that

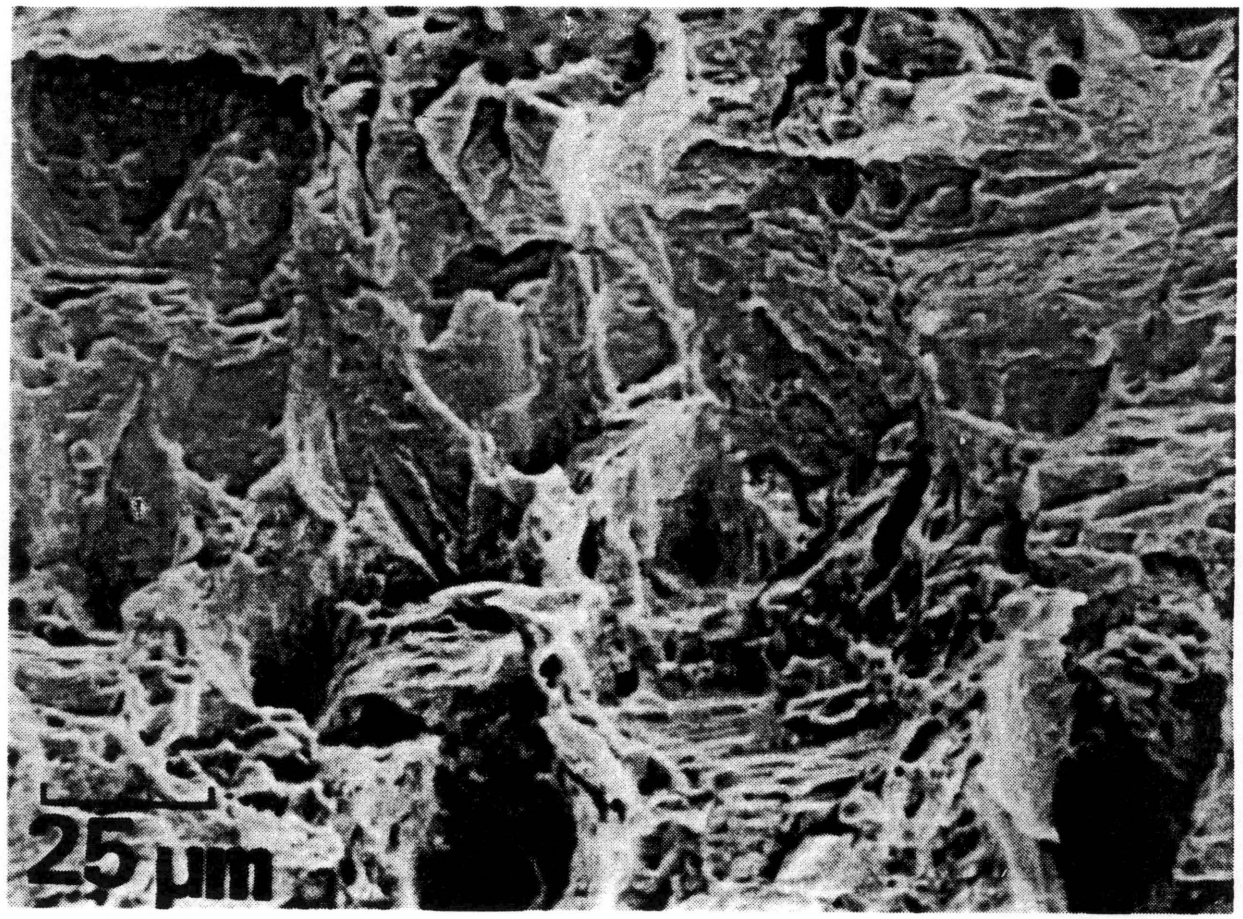

Figure 15. Fractograph of hydrogen charged 304L sample tested at 25°C in slow bend mode.

stacking fault energy and coplanar dislocation motion are of primary importance (32). Strain induced transformation to α' marteniste is unlikely in 21-6-9 stainless steel, but the effect of stacking fault energy and coplanar dislocation motion may be very important to discussion of hydrogen effects on this alloy. The low stacking fault energy associated with 21-6-9 and 304L stainless steels causes these materials to form coplanar dislocation arrays during the early stages of plastic strain. Thus, plastic deformation leads to dislocation pile-ups at grain boundaries, second phase particles and other obstacles. These pile-ups cause localized stress concentrations. Furthermore, large lattice dilations will develop at the tip of the pile-up and the hydrogen concentration at that area will increase as hydrogen laden dislocations accumulate. This accumulation requires both plastic deformation and hydrogen diffusion and can explain the effect of hydrogen and strain rate on the fracture of these two austenitic steels tested in this program.

4.11 21-6-9 Stainless Steel

The slow bend tests conducted at 25°C will be used as a detailed example to illustrate the interrelationship between hydrogen content, fracture mode, energy absorbed and dislocation motion. As mentioned previously, the 2000 psi charged samples exhibited a mixed mode fracture of microvoid coalescence/faceted fracture while the as-received samples showed microvoid coalescence type fracture. A larger hydrogen induced fracture transition was observed in the 20,000 psi charged samples, which were much more faceted than the samples charged at 2,000 psi. Changes in fracture mode accompanying hydrogen charging are well documented (16). Rationale for such a transition begins by requiring that a critical hydrogen concentration develop at an interface and promote failure of that interface. When this critical hydrogen concentration is reached the interfacial strength will be lowered to the point that interfacial fracture will occur before further plastic strain can develop. Verification of such interfacial weakening is seen in Table 5, whereby increasing the hydrogen charging pressure increases the degree of faceted fracture associated with a given sample. This transition to a more brittle fracture with increasing hydrogen content is reflected in a large decrease in energy absorbed because the ability of the sample to

Table 5

Fracture Features Observed in Stainless Steel

Charging	Impact Fracture	Slow Bend Fracture
21-6-9 Stainless Steel		
Temperature: 25°C		
0	Dimpled Rupture	Dimpled Rupture
2 ksi	Dimpled Rupture	Dimpled Rupture and Faceted
20 ksi	Dimpled Rupture	Dimpled Rupture and More Faceted
Temperature: -197°C		
0	Dimpled Rupture and Faceted	Faceted
2 ksi	Dimpled Rupture and Faceted	Faceted
20 ksi	Dimpled Rupture and More Faceted	Large Well Defined Facets
304L Stainless Steel		
Temperature: 25°C		
0	Dimpled Rupture, Two Dimple Sizes	Dimpled Rupture
2 ksi	Dimpled Rupture, Larger Dimples	Dimpled Rupture and Facets
20 ksi	Dimpled Rupture, Much Larger Dimples	Facets and Some Dimpled Rupture
Temperature: -197°C		
0	Dimpled Rupture, Two Dimple Sizes	Dimpled Rupture, Two Dimple Sizes, More Finer Dimples than Impact Samples
2 ksi	Dimpled Rupture, Two Dimple Sizes	Dimpled Rupture, Two Dimple Sizes
20 ksi	Dimpled Rupture, Two Dimple Sizes	Dimpled Rupture, Two Dimple Sizes

plastically strain is decreased. In contrast, the impact tested samples of 21-6-9 stainless steel tested at room temperature failed by ductile rupture regardless of charging conditions. This result coupled with the large scale effects observed in the slow strain rate tests is consistent with the assumption that dislocation transport of hydrogen increased the hydrogen content at the typical interface. As the strain rate increases from slow bend to impact tests the amount of hydrogen transported by dislocations decreased and the amount of embrittlement decreased. Thus, there is a justifiable absence of a hydrogen induced change in the fracture mode for impact tests at room temperature. The only observable hydrogen effects were enhancement of microvoid nucleation and growth and a slight hydrogen induced reduction in the energy absorbed at fracture. The fact that some hydrogen induced effects were observed in the impact tests shows that hydrogen segregation to pre-existing sites prior to testing in austenitic steels can cause embrittlement and that dislocation transport is not a necessary prerequisite for embrittlement.

When tests were conducted on uncharged 21-6-9 stainless steel at liquid nitrogen temperature, slow bend test samples exhibited faceted fracture and impact test samples exhibited a dimple rupture fracture with some interfacial fracture apparent. The major hydrogen effect was to increase the degree of faceted fracture. This increase was greatest in slow bend tests samples charged to 20,000 psi and these samples also showed the largest losses in energy required to cause fracture.

4.12 304L Stainless Steel

Many of the same observations and arguments presented for hydrogen effects on 21-6-9 stainless steel apply to tests conducted on Type 304L stainless steel. Increasing the hydrogen charging pressure increased the typical microvoid size in the dimple rupture fracture of impacted tested samples at room temperature. Justification for this hydrogen induced effect is that the critical hydrogen concentration for significant weakening of continuous boundaries is not achieved, thus very little interfacial fracture is observed. Hydrogen absorption does, however, cause early microvoid nucleation and promotes easy growth by lowering the strength of particle-matrix interfaces and by the continual "dumping" of hydrogen into the void during plastic strain. The hydrogen induced effects on ductile failure process in stainless steels tested in tension have been described in

a similar manner (33).

The fracture surface of 304L samples tested at a slow strain rate at room temperature showed some facets in charged samples. The appearance of faceted fracture in hydrogen charged slow bend samples again emphasizes the importance of dislocation transport of hydrogen in promoting hydrogen induced fracture transitions while the observed hydrogen induced effects in the impact tests continue to demonstrate that such transport is not necessary for hydrogen embrittlement to occur.

It is interesting to note that in tests of 304L samples at liquid nitrogen temperature, all fractures were ductile rupture regardless of strain rate. However, there were two distinct microvoid sizes in most samples. Large microvoids are surrounded by areas of much finer microvoids. In slow bend tests, the overall size of the voids is larger, probably due to a greater hydrogen concentration in the voids achieved by increased dislocation transport of hydrogen at the slow strain rates. Such a result is consistent with the hypothesis that hydrogen promotes microvoid nucleation and growth. The enhanced growth could be due to the increased pressure in the void (as preveiously suggested) or due to strain localization because of the hydrogen concentration gradients. This result is supported by the observation of increased void size with an increase in hydrogen charging from 0 to 20,000 psi.

The observation of increased interfacial fracture and an increased ease for microvoid nucleation and growth in 21-6-9 and 304L stainless steels as the hydrogen charging pressure increases is consistent with a model of hydrogen assisted changes in fracture mode (17) (Figure 16). In this model, changes in the failure mode are related to hydrogen concentration, flow stress and interfacial strength. Hydrogen is thought to raise the flow stress and lower the interfacial strength of austenitic stainless steel and the results of this study clearly support the lowering of interfacial strengths. Thus, as indicated by Figure 16, low hydrogen concentrations will cause ductile failure and high hydrogen concentrations will induce interfacial fracture for a given test. The value $[H_c]_1$ represents the critical hydrogen concentration for the onset of interfacial fracture and $[H_c]_2$ represents the critical hydrogen concentration for a purely interfacial fracture. The failure model described by Figure 16 allows rationalization of the results of the present study. For example, in 21-6-9 samples tested at room temperature, a fracture transition from dimpled rupture to faceted/dimpled to interfacial fracture was observed when the hydrogen charging pressure was increased (Figure 13). This transition is qualitatively predicted from the decreasing interfacial strength shown in Figure 16. Furthermore, the fact that such a fracture transition was not observed in 304L stainless steel is also predictable because the flow stress in this

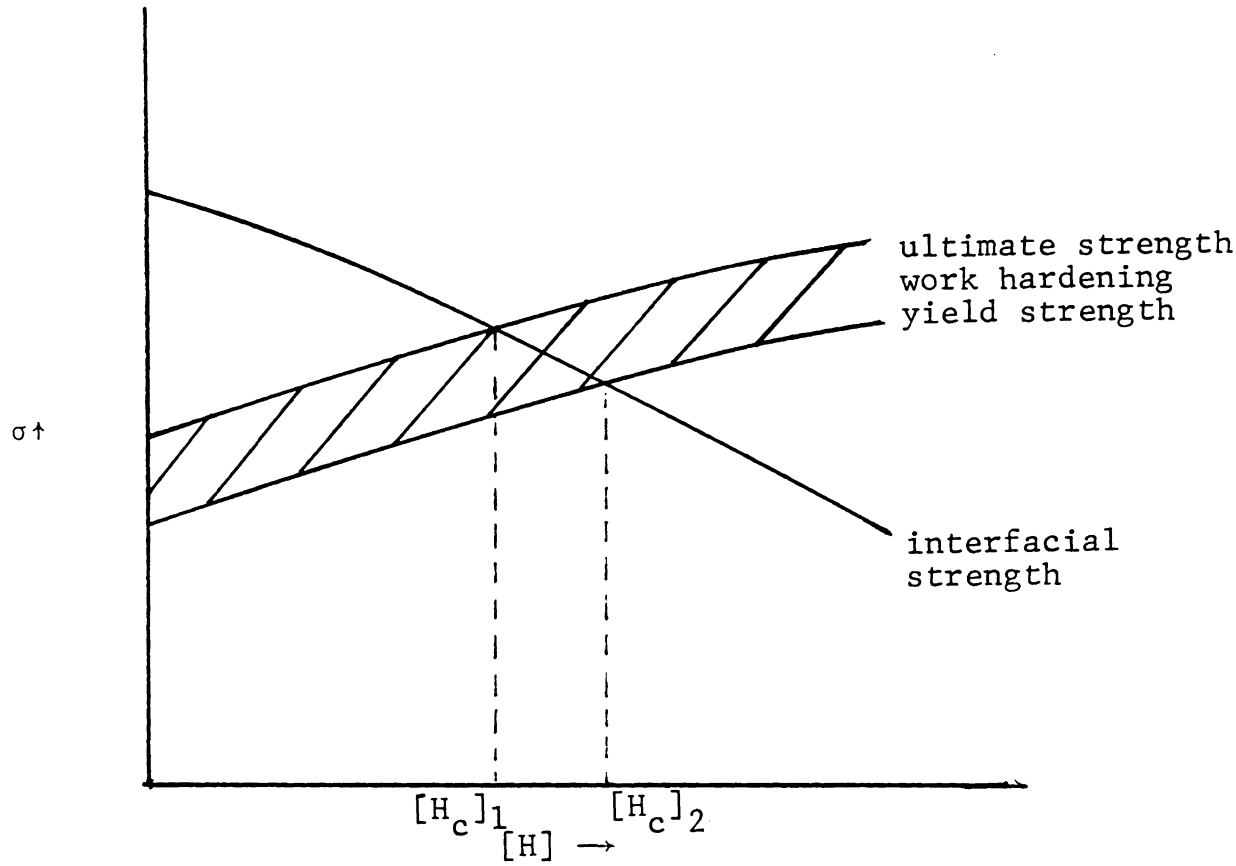

Figure 16. Model to account for hydrogen assisted changes in fracture mode.

material is less than that for 21-6-9. Thus, the flow stress curve does not intersect the interfacial strength curve. This lower flow stress was therefore the cause of the lack of interfacial fracture in the 304L samples which were tested under the most severe embrittling conditions, although a small amount of faceted fracture occurred in isolated areas (Figure 15).

These combined results show that the role of hydrogen in the embrittlement of austenitic stainless steels is to lower the strength of various interfaces. Other work at VPI (34) has shown that twin boundaries are the most easily embrittled interface, then grain boundaries and slip bands. Both steels tested in this study had low stacking fault energies, and therefore contained numerous annealing twins. The observation of hydrogen induced facted fracture in the samples tested under impact loading demonstrates that dislocation transport of hydrogen is not necessary to cause embrittlement. However, the fact that slow bend testing enhances embrittlement demonstrates that hydrogen relocalization during testing (dislocation transport) contributes to the embrittlement process. Therefore, these studies show that interfacial weakening by hydrogen absorption occurs because of hydrogen segregation to pre-existing sites and that the extent of this weakening increased as the hydrogen content is increased. Increases in hydrogen content take place whenever the sample is either exposed to increasing

hydrogen pressures or tested at slow strain rates which cause dislocation transport of hydrogen.

4.2 Mild Steels

4.21 Monotonic Testing

Previous monotonic hydrogen testing of AISI 1015 steel in a burst rupture assembly showed that the type of rupture (leak or burst) associated with overpressurization to failure was dictated by the surface finish on the test sample (35). The two types of failures commonly associated with overpressurization are illustrated in Figure 17. It was noted that, in general, samples with a relatively rough surface finish failed by leaking, while those with a relatively smooth surface finish failed by bursting when overpressurized with hydrogen gas. The majority of samples tested in oxygen failed by bursting. Such a failure transition was justified by assuming that hydrogen is absorbed during testing and that the absorbed hydrogen promotes strain localization and lowers the interfacial strength at the tip of large scratches or flaws in samples. The size of the flaws is a function of surface finish and rough surfaces allow for increased adverse hydrogen effects. If this is the case, hydrogen enhances flaw growth from the tips of large scratches and causes a crack to penetrate the sample resulting in a leak-type failure. However, in samples with a smooth surface finish, it was assumed that surface scratches created by the grinding/polishing operation were

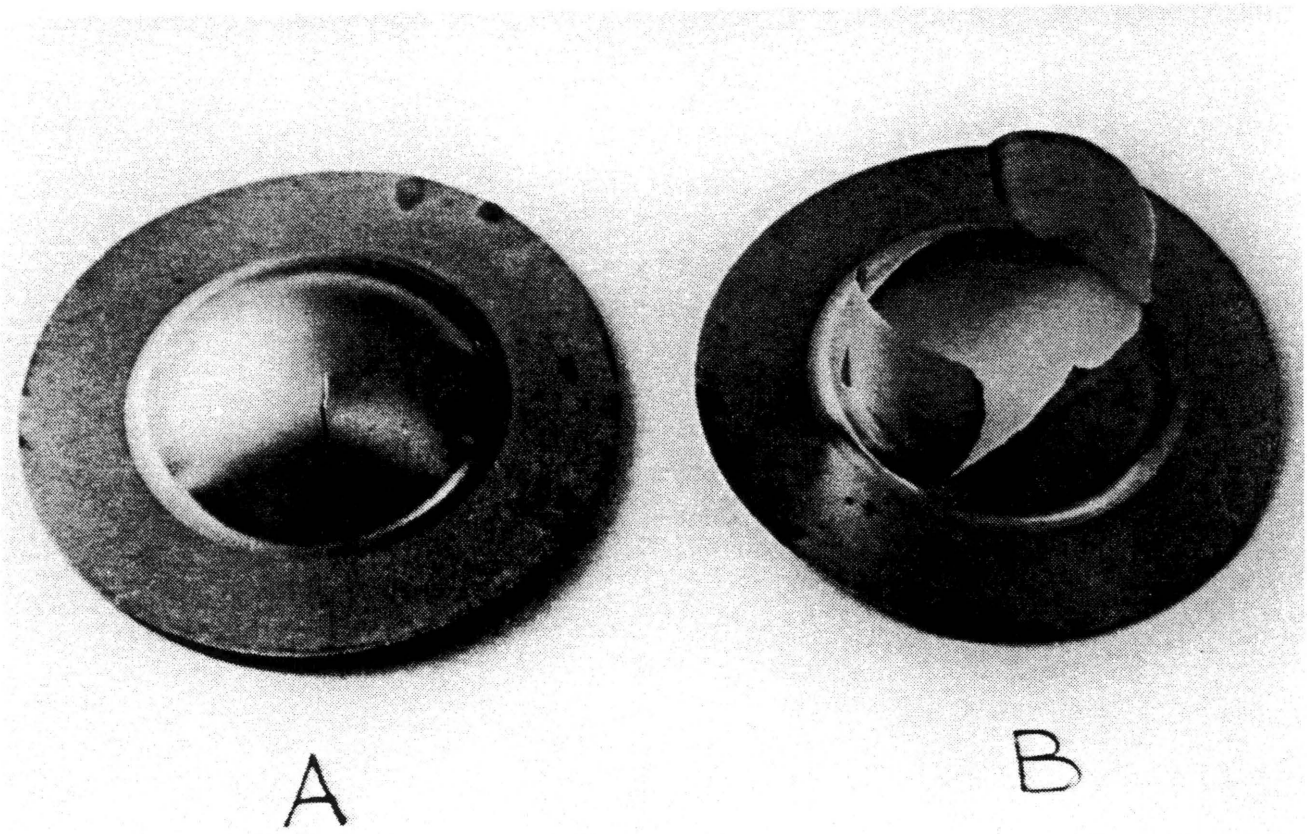

Figure 17. Two types of failures associated with over-pressurization of mild steels: A) leak and B) burst.

not large enough to promote hydrogen assisted strain localization and interfacial weakening, and therefore hydrogen induced flaw growth was not observed. Thus, unstable crack growth did not occur, no crack penetrated the sample and a burst-type failure resulted. These observed changes in failure mode are consistent with the results of impact and slow bend tests on stainless steels, Section 4.1, which showed an increased tendency for brittle interfacial fracture with increased hydrogen charging pressure. Notch or scratch tips which serve to concentrate the stress also serve to increase the local hydrogen concentrations because of the well established tendency for hydrogen to segregate to regions of high triaxial stresses.

A companion study was conducted with AISI 1018 steel samples and did not yield results which were obviously consistent with the results from 1015 steel. For example, during initial hydrogen testing of the AISI Type 1018 steel disks, eleven out of twelve samples failed by leaking regardless of surface finish. Similar tests conducted in oxygen all resulted in burst-type failures.

Surface topography studies and metallographic investigations were conducted on 1015 and 1018 steels to determine what variables were causing hydrogen effects in 1018 steel samples to differ from those previously observed in 1015 steel. Surface profilometry scans to characterize the various surface finishes revealed that, as expected, the

surface roughness of samples became less as they were progressively ground with finer grit paper and alumina polish. Qualitative analysis of the five largest peaks from various surface finishes are presented in Table 6, along with an example of a typical profilometry scan in Figure 18. Tests conducted on 1015 steel disks yielded a characteristic roughness number of 2.1 μm (400 grit) or higher for the samples which leaked and .39 μm (600 grit) or lower for the samples which burst when tested in hydrogen. Similar surface roughnesses were observed on the 1018 steel samples but no change in failure mode from leak to burst was observed, thus the lack of a fracture transition was not attributed to differences in surface finish. However, metallographic examination of both materials revealed relatively large inclusions strung out in the rolling direction of the 1018 steel. Such inclusions were not apparent in the 1015 steel. Because of the importance of hydrogen localization at interfaces such as twins, grain boundaries and second phase particles (34), and because of the potential for embrittlement of the inclusion-matrix interface the inclusion stringers were believed to be influencing the nature of the hydrogen embrittlement processes in 1018 steel disks. Support for this conclusion was found by determining the average width of inclusions in samples which leaked in hydrogen was greater than 2 μm. This "roughness" approaches the

Table 6

Peak to Peak Value of Surfaces Scanned

	240 Grit	320 Grit	400 Grit	600 Grit	1 μm Polish	.05 μm Polish
Peak to Peak Values	6.2 μm	2.2 μm	1.5 μm	.32 μm	.23 μm	.08 μm
	7.4	2.6	2.0	.64	.29	.10
	5.8	2.0	2.3	.34	.20	.12
	4.7	2.5	2.7	.36	.23	.10
	5.2	2.5	2.2	.30	.25	.12
Average	5.9	2.4	2.1	.39	.24	.10

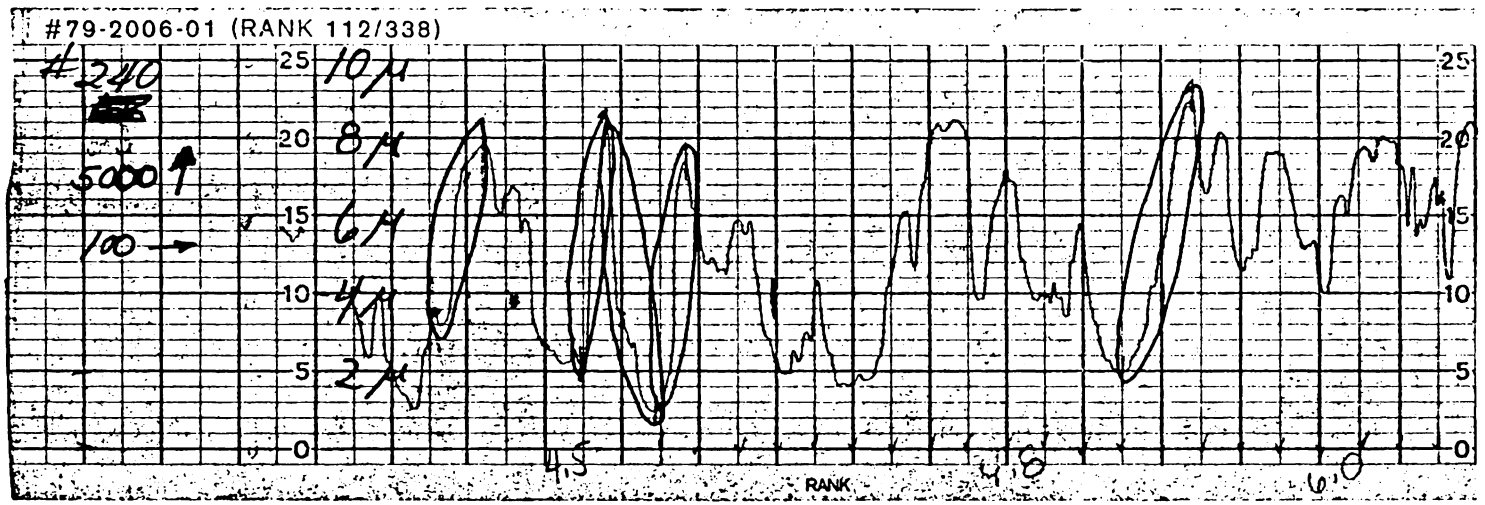

Figure 18. Surface Profilometry Scan of Sample with #240 Grit Finish. The Five Largest Peaks are Circled.

characteristic roughness number (2.1 μm) for a fracture transition in 1015 steel disks. Therefore, if inclusions serve as possible initiation sites for hydrogen induced fracture, the surface finish controlled fracture transition in "clean" 1015 steel should not be observed in the inclusion dominated 1018 steel. Hydrogen effects on the relatively large inclusions would override surface finish effects and hydrogen enhanced flaw growth would be observed.

To establish the role of inclusions in the hydrogen embrittlement process, as-received disks of 1018 steel with various inclusion sizes were pressurized (strained) at selected rates to failure in both hydrogen and oxygen gasses. Results are presented in Figure 19. For samples tested in oxygen, pressurization rate had little effect on the failure pressure or failure mode. In test times from 8 seconds to over 40 hours, all samples failed by bursting at approximately 1250 psi, with only one exception. Fractographic studies on selected samples revealed that the inclusion-matrix interfaces served as microvoid nucleation sites, but these nucleation sites did not cause premature failure. However, 1018 steel samples pressurized with hydrogen showed a significant decrease in rupture pressure as the pressurization rate decreased (Figure 19). Furthermore, the test samples could be divided into two distinct groups. One

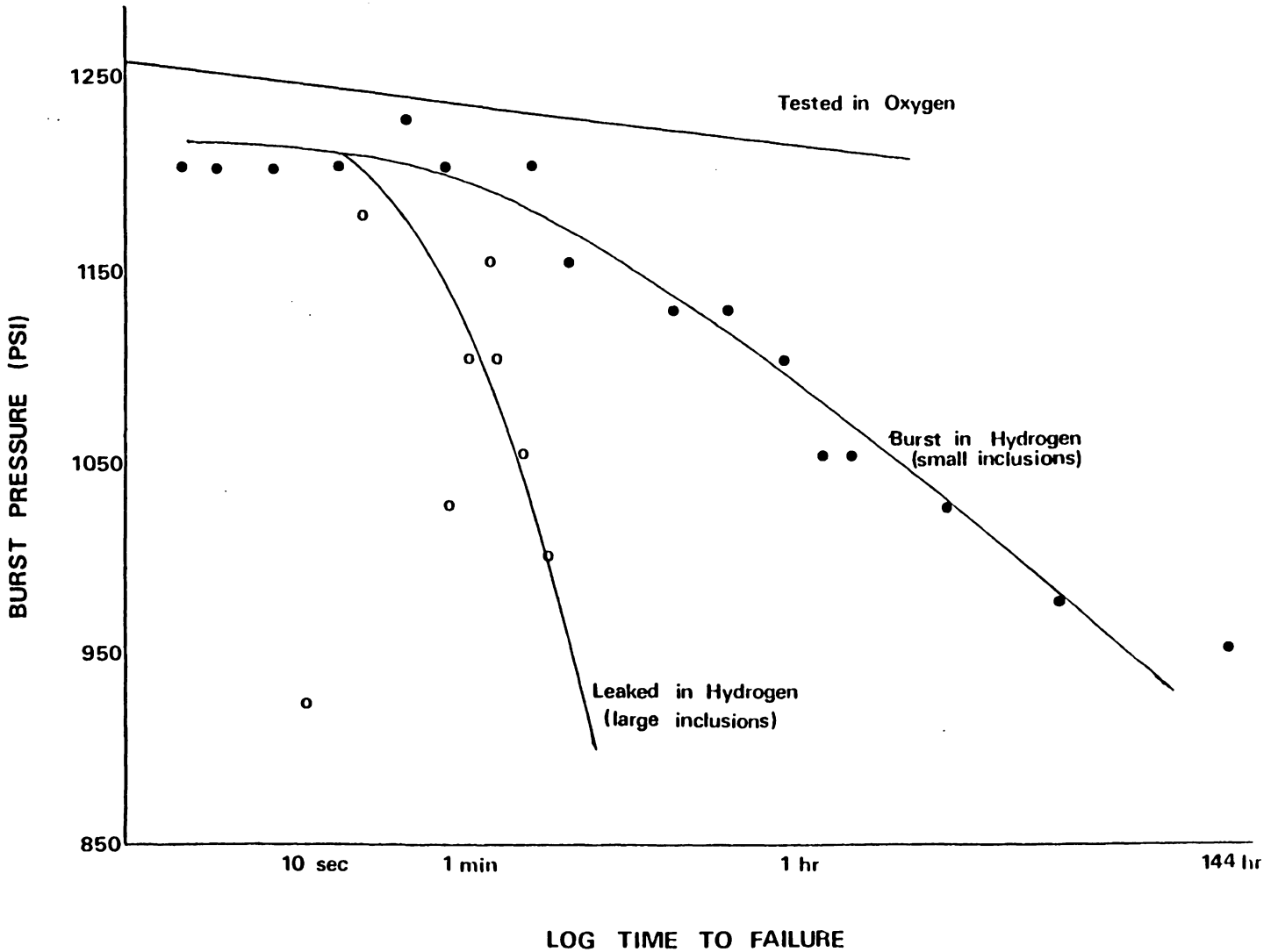

Figure 19. Results of Burst Rupture Tests on AISI 1018 Steel.

group of samples failed by bursting at hydrogen pressures much higher than samples in the other group which generally failed by leaking. Metallographic examination of the two groups revealed that in samples which leaked, the groupings of inclusions in stringers and the stringers themselves were much larger than in samples which burst (Figure 20). This result emphasized the importance of metallographic features in hydrogen embrittlement. Fractographic studies of samples in both groups showed that the inclusion-matrix interfaces served as failure initiation sites and growth of these crack-like voids resulted in final fracture of the sample. (Figure 21). Such a result is in agreement with work on A-106 steel which showed that hydrogen weakens inclusion-matrix interfaces and thus inclusion orientation has a major influence on crack nucleation and growth (20).

The rationale for the observed hydrogen effects on 1018 steel assumes that hydrogen segregates to the high stress region of the inclusion-matrix interface and causes a reduction in the interfacial energy. This enables lenticular voids to develop around inclusions during plastic deformation in the presence of hydrogen. Such an effect was most pronounced when the inclusion groupings were large and the pressurization rate was slow. Furthermore, under these conditions the primary fracture mode near the cracked region was quasi-cleavage (Figure 22) which is typical of

Figure 20A

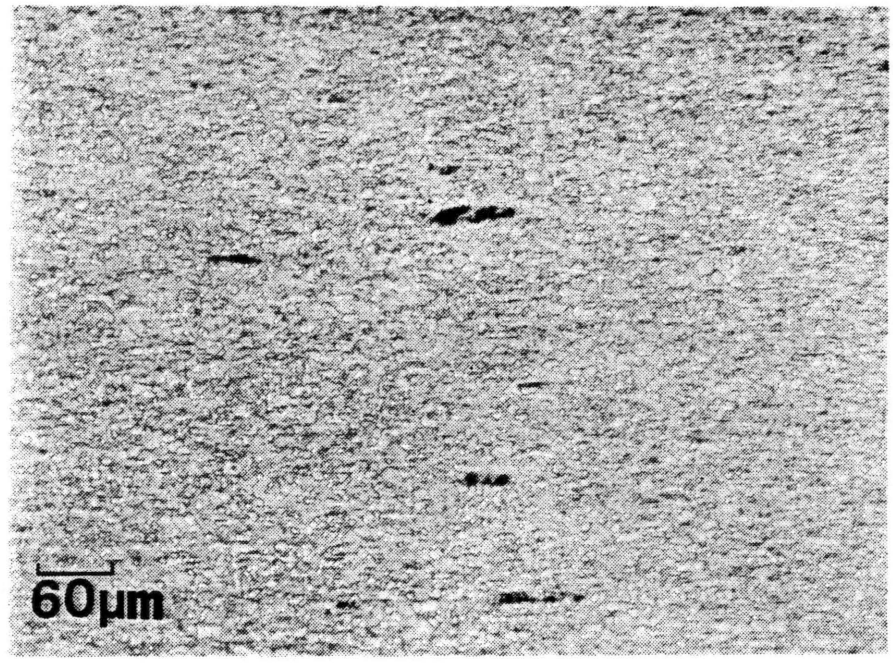

Figure 20B

Figure 20. Micrographs of 1018 disk rupture samples: 20A) large stingers of of inclusions in sample which leaked and 20B) small stringers of inclusions in sample which burst.

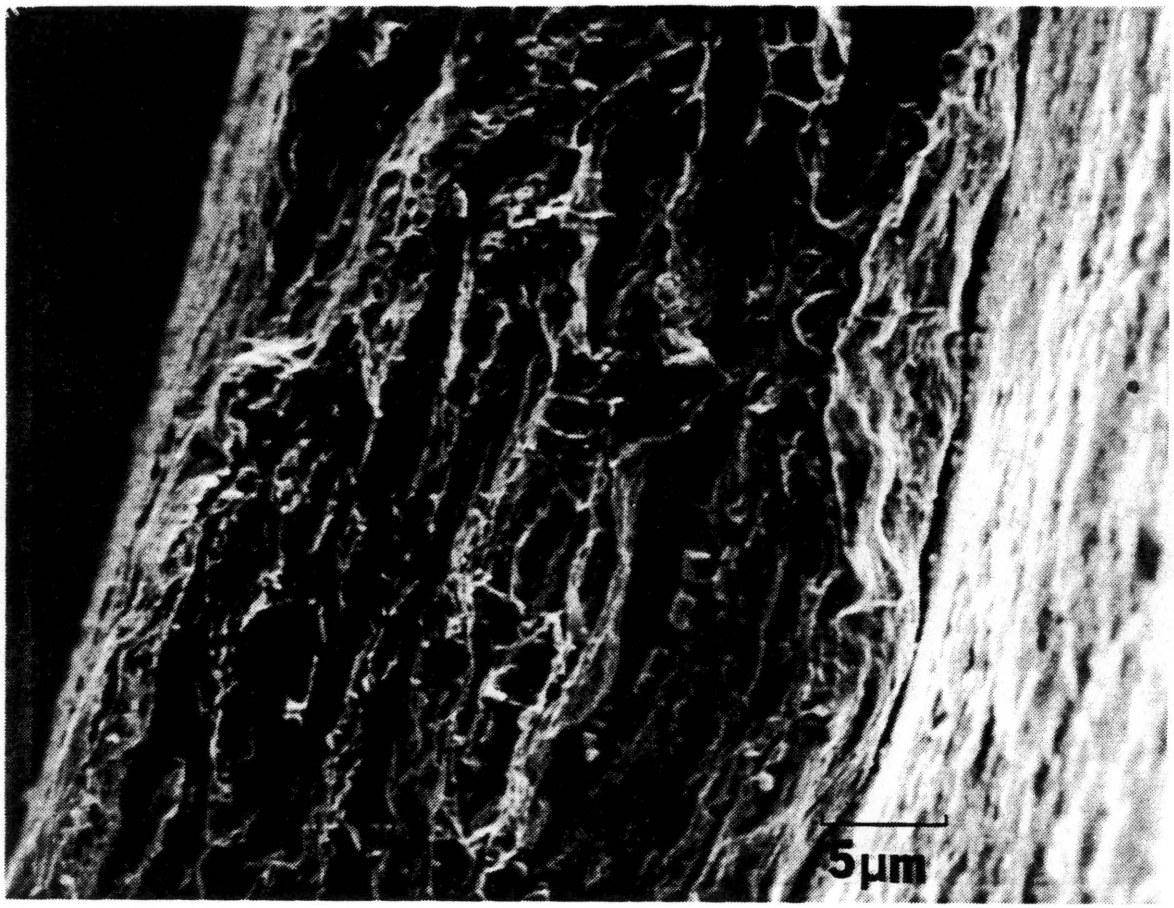

Figure 21. Fractograph of crack-like void in hydrogen tested 1018 steel sample.

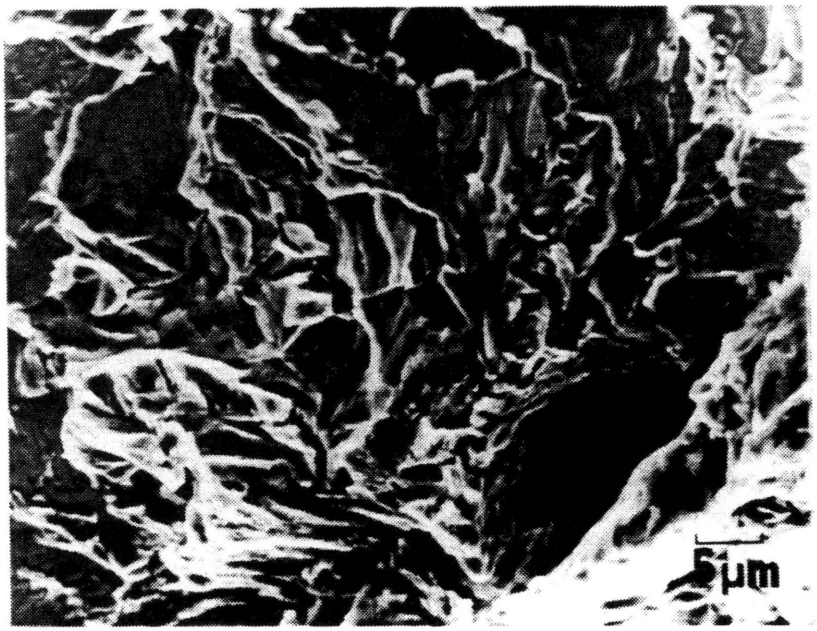

Figure 22. Fractograph of hydrogen tested 1018 steel sample.

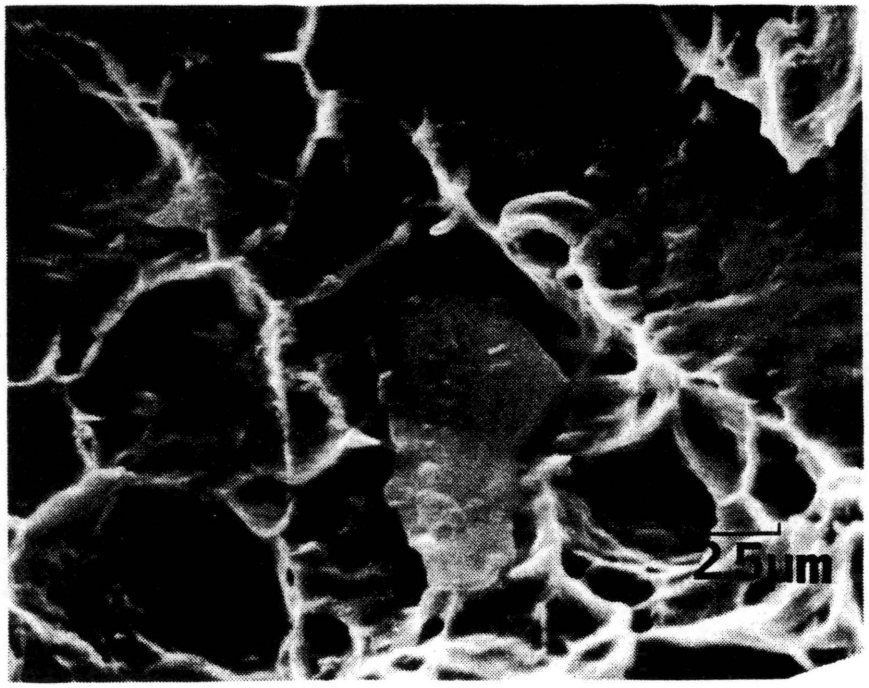

Figure 23. Fractograph of oxygen tested 1018 steel sample.

hydrogen induced cracking of mild steels and has been noted by other investigators as evidence of hydrogen suppression of the ductile process (36). However, when inclusion groupings were small and/or the pressurization rate was fast, the failure mode was primarily microvoid coalescence (Figure 23). This lack of hydrogen induced effects demonstrates the time dependent nature of hydrogen embrittlement and the importance of metallographic features in relation to hydrogen induced fracture. These two characteristics were also typical of the results from the tests of austenitic steels.

This study thus emphasizes the importance of hydrogen at interfaces and the results are compatible with decohesion-type mechanisms for hydrogen embrittlement, but in this case the decohesion is occurring at interfaces rather than in the matrix. Co-workers have indirectly verified the results of this study through hydrogen diffusivity measurements (37). Tests were conducted with 1018 steel samples from the same stock as the disk rupture samples, and the diffusivity of hydrogen through the membrane was shown to decline with time. The decline of diffusivity is explained by assuming that atomic hydrogen segregates to the inclusion-matrix interface, recombines at the interface to form hydrogen gas which stresses the interface by pressurization and causes the interface to fail. Thus, diffusivity will decline with time due to void growth around inclusions and the irreversible

trapping associated with this void. This result further emphasizes the importance of interfaces in both embrittlement and transport processes.

4.22 Acoustic Emission Testing

To qualitatively determine the nature of crack growth in these mild steel samples exposed to gaseous hydrogen acoustic emission measurements were made. The majority of previous studies using acoustic emission to determine hydrogen enhanced crack growth have been conducted on high strength steels (38) because these metals have been shown to be very susceptible to hydrogen induced cracking. Other investigators have observed that acoustic emission signals are generated during hydrogen induced cracking of cathodically charged metals (39). Thus, although a data base was available for acoustic emission studies, little information was available for such tests on mild steels.

Acoustic emission events evolve from the energy released from a material by the plastic deformation or fracture processes (40). In the present study, preflawed samples of 1015 steel were tested in the disk rupture assembly with the intention of monitoring crack growth from the artificial flaw. Acoustic emission events eminating from the advancement of a crack are easily distinguished from other acoustic emission events because they tend to have the most energy and thus have the largest amplitude. This high energy

release accompanying microcrack formation is attributed to the large number of dislocations required to form a crack Therefore, high amplitude cracking events are easily differentiated from low energy events which also produce new surface by phenomenon such as slip deformation. However, to ensure that the acoustic emission events monitored originated from crack advancement and not from plasticity effects, a straight tensile test was conducted on 1015 steel using the acoustic emission monitoring system, Figure 24. In this test, there was a continuous acoustic emission signal generated, typical of plastic deformation of steels (41). No discrete large scale acoustic emission events were associated with the tensile test. This observation was used to verify that any discrete, large scale acoustic emission events generated in the disk rupture tests would be from microcrack advancement and not plasticity effects.

Three test gases (O_2, commercial H_2 and high purity H_2) were used to study the crack growth behavior in 1015 steel disk samples prepared with various artificial flaws (indentations with the Rockwell C hardness indentator using 60, 100 and 150 kg loads). The majority of experiments were conducted on samples with a 60 kg flaw and the discontinuous nature of crack growth in samples tested in either of the hydrogen environments was obvious in more than 100 different tests. Results from these tests on 60 kg flawed samples

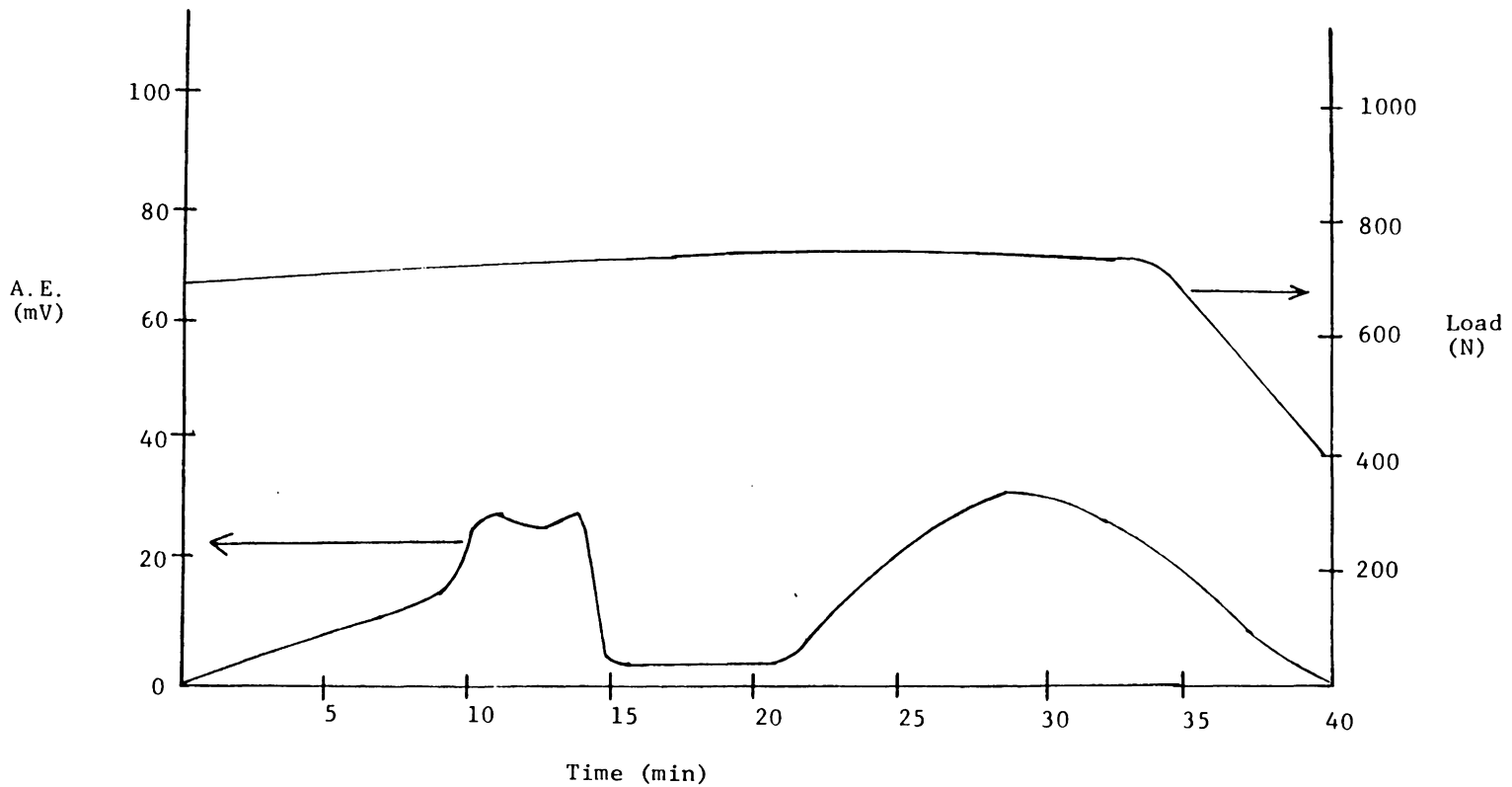

Figure 24. Acoustic Emission From Tensile Test of 1015 Steel.

showed no obvious hydrogen embrittlement effects (crack growth) below 700 psi. However, the failure pressure of samples tested in hydrogen ($\sim$ 1500 psi) was lower than the failure pressure of equivalent tests conducted in oxygen ($\sim$ 1575 psi). This result is in agreement with earlier work which found a significant reduction in the failure pressure of steel disks which were monotonically pressurized with hydrogen (36). The chart recordings of acoustic emission samples tested in hydrogen exhibit several high amplitude bursts each followed by a "quiet" period (Figure 25). These discrete acoustic emission bursts were attributed to discontinuous crack growth originating from the artificial flaw. Companion experiments conducted in oxygen showed no evidence of high amplitude acoustic emission bursts, Figure 26.

Fractographic studies on representative samples failed in hydrogen and oxygen support the conclusion that crack growth in hydrogen was discontinuous. Failure of the hydrogen tested samples were primarily by quasi-cleavage The discontinuous nature of crack growth was apparent in the stepwise nature of the crack front (Figure 27). Furthermore, it has been observed in several hydrogen tested samples that there is a strong correlation between the number of crack fronts and the number of high amplitude events observed from acoustic monitoring (compare Figures

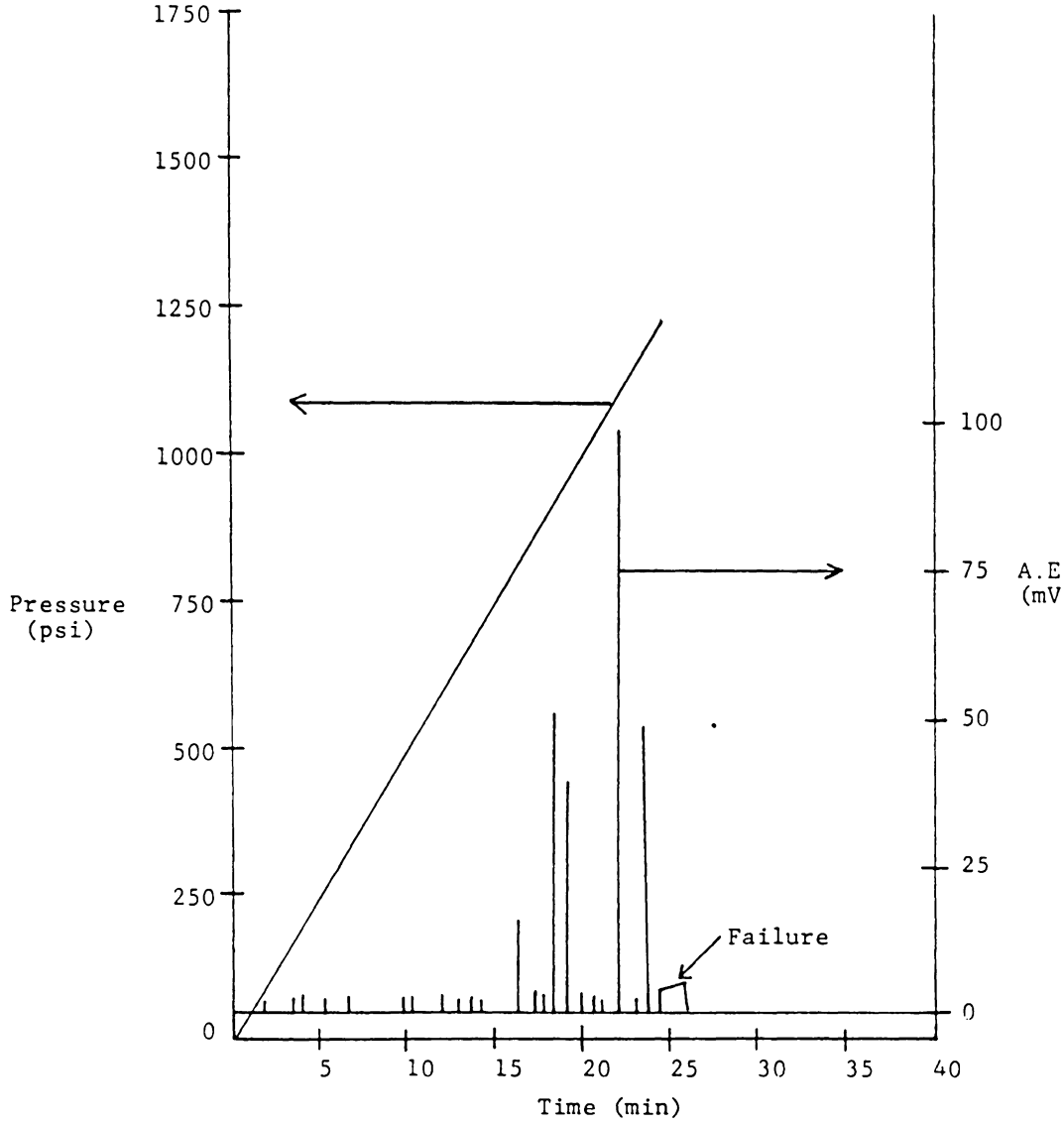

Figure 25. Acoustic emission of hydrogen tested 1015 sample showing discrete high amplitude events.

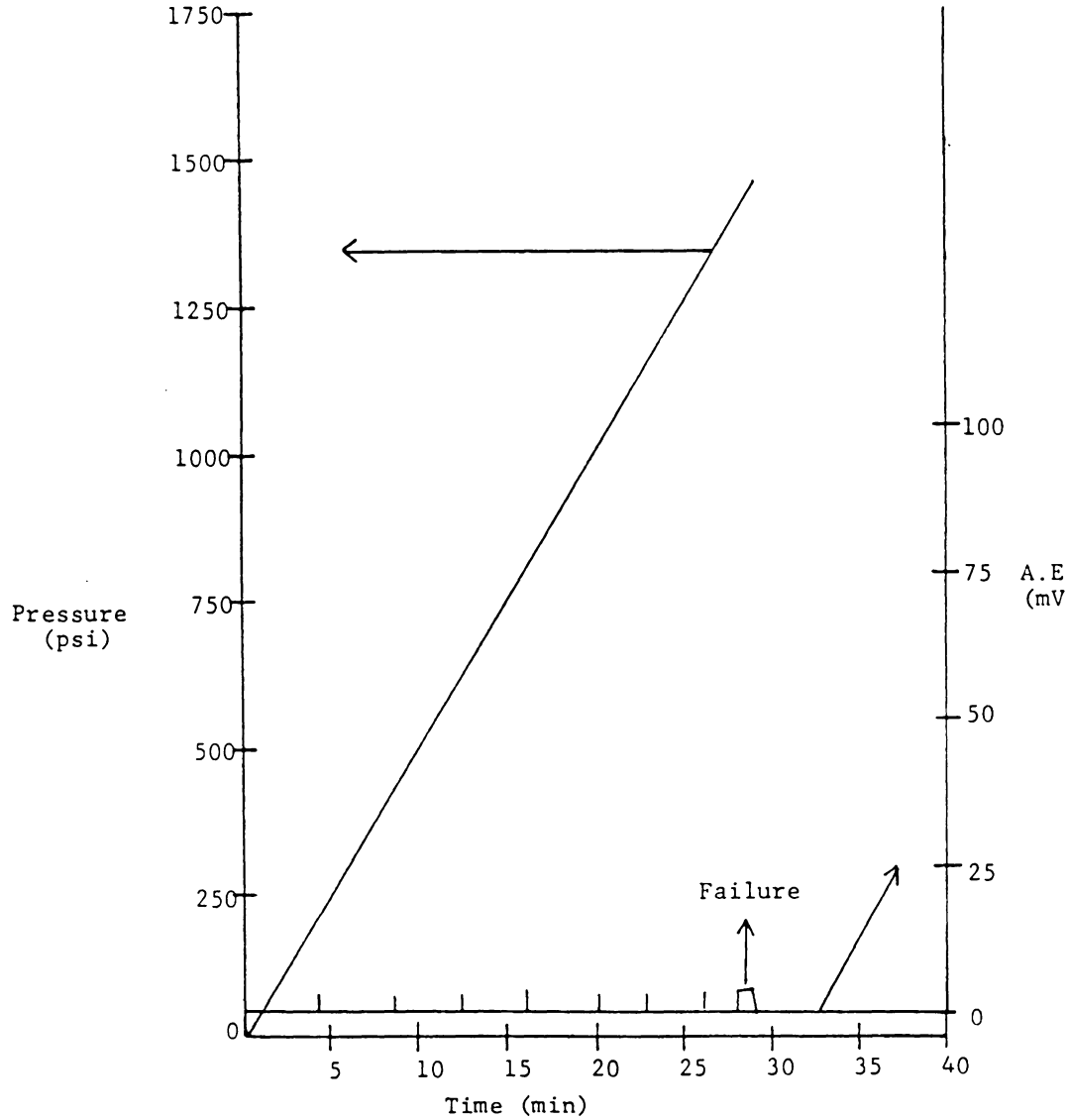

Figure 26. Acoustic emission of oxygen tested 1015 sample showing no high amplitude events.

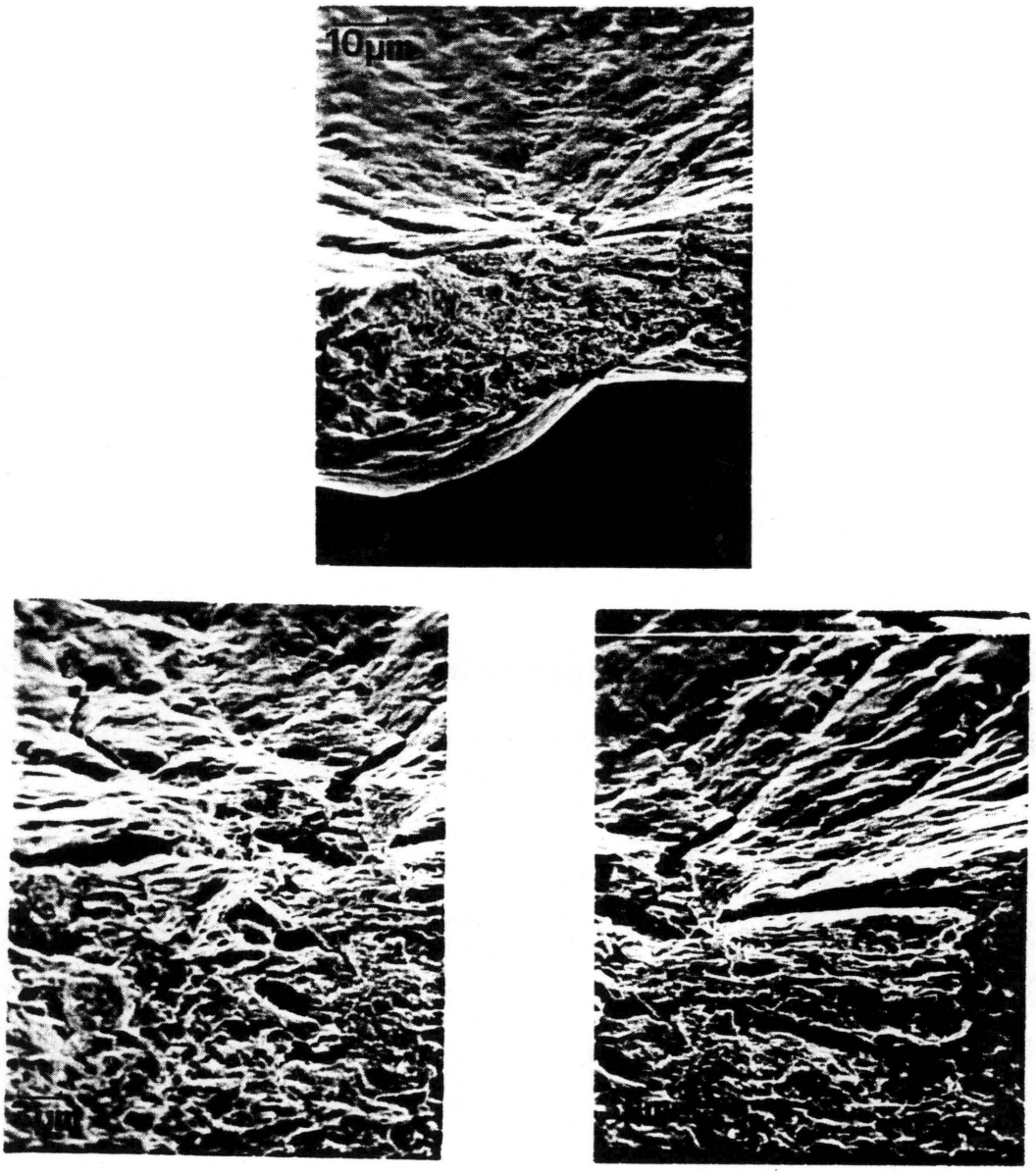

Figure 27. Fractographs of stepwise crack growth in 1015 steel sample tested in hydrogen.

25 and 27). However, samples failed in oxygen had a primarily microvoid coalescence type failure and did not exhibit any high amplitude acoustic emission events.

The change in fracture mode from microvoid coalescence to quasi-cleavage for samples tested in hydrogen has previously been reported. This change in fracture mode explains the high amplitude acoustic emission bursts observed in hydrogen tested samples because discrete, high energy acoustic emission signals are associated with interfacial fracture and microcrack advancement. These observations suggest that hydrogen absorbed during the test weakened interfaces and promoted interfacial decohesion.

The discontinuous nature of crack growth in hydrogen tested samples has previously been seen through acoustic emission monitoring of cathodically charged high strength steel (39). Dunegan and Tetelman attributed the "quiet" period between large acoustic emission bursts as the time for hydrogen to diffuse to the tip of the advancing microcrack. In the present investigation, this quiet period corresponds to the time required for either diffusion or dislocation transport of hydrogen to cause the local hydrogen concentration at crack tip to reach the level required for crack advance.

A secondary observation evolved from this study indicated the importance of hydrogen test gas purity and flaw size on embrittlement. As mentioned previously, two

grades of hydrogen gas were employed. The as purchased grades were commercial and high purity but no determinations of the actual purity of the test gases were made. In the majority of tests conducted, the failure pressure of samples tested with a 150 kg flaw was significantly higher in high purity hydrogen than in comparable tests conducted in commercial hydrogen. This result is an apparent contradiction to previously conducted studies which saw an increase in hydrogen effects as the hydrogen gas purity increased (7). One possible explanation for such an occurrence is that the commercial hydrogen (specified as 98-99% pure) was, in reality, of higher purity than the high purity gas (specified as 99.995% pure). Since only 15 tests were conducted under these conditions, more tests are needed to establish the role of gas purity in this hydrogen embrittlement process.

Further investigation of samples with a 150 kg flaw showed that failure occurred by a leak and the leak always occurred through the artificial flaw when tests use the high purity hydrogen. When commercial hydrogen was used no one mode dominated the failure process and the failure generally occurred a very small distance away from the artificial flaw (Figure 28). An explanation for such an occurrence has not been established and needs to be studied in future research.

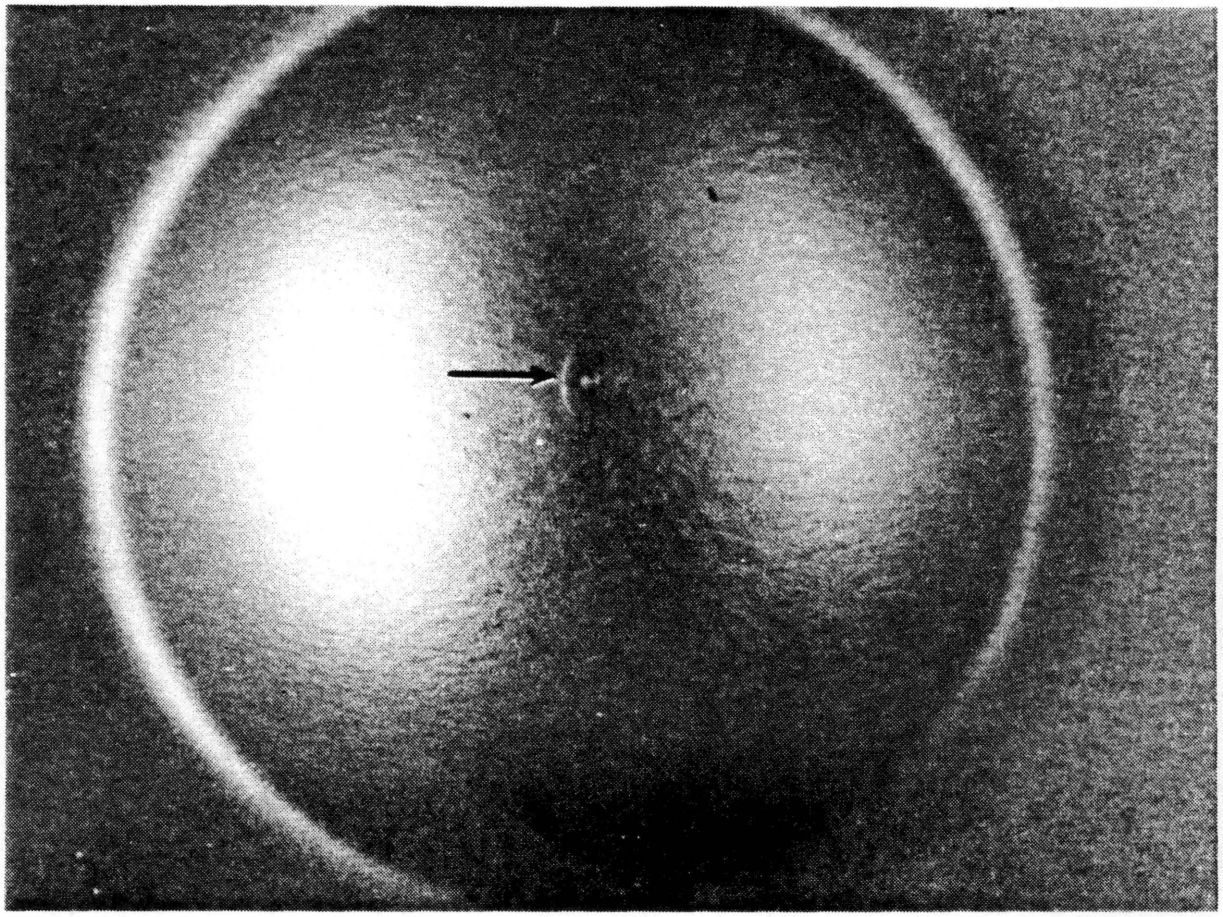

Figure 28. Disk rupture sample tested in hydrogen showing failure occurring a small distance away from the artificial flaw.

These studies with mild steel samples support the stainless steel studies in showing that hydrogen embrittlement processes occur primarily by hydrogen induced interfacial weakening. The studies also suggest that the hydrogen concentration at the interface must reach some critical level for embrittlement and that once that level is reached rapid fracture takes place at the weakened interface. Additionally, the data show that hydrogen concentrations at interfaces can increase during testing and that this test induced change in hydrogen level is strain rate dependent.

4.3 Aluminum

Many investigations of environmental effects on high strength aluminum alloys have been concerned with hydrogen (or moisture) assisted fatigue crack growth (26). There is general agreement that moisture significantly increases the fatigue crack growth rate because of hydrogen absorption, but the mechanism by which this occurs is unclear. In most studies such an effect has been attributed to the presence of internal hydrogen, hydrogen transported by dislocation and the formation of an oxide film which prevents hydrogen out-gassing.

A series of tests on the effect of humidity on the torsional fatigue life of 2024-T3 (peak aged) aluminum (42) showed that no change in the fatigue life resulted unless

there was an accompanying reduction in the hardness of the specimen. It was therefore postulated that hydrogen absorption during fatigue was altering the aging characteristics of 2024 aluminum causing localized softening. This local softening was assumed to be caused by hydrogen effects on the developing interface in the precipitation hardenable aluminum alloy. This assumption was based on the fact that hydrogen has been shown to alter the age hardening characteristics of 15-5 pH stainless steel (43). In the 15-5 steel study, it was observed that the hardening kinetics were faster when samples were annealed in hydrogen than when annealed in argon or dry air. Little or no literature exists on the effect of hydrogen on the age hardening characteristics of aluminum alloys. To date, most investigators agree that hydrogen does embrittle aluminum, but most studies have been concerned with hydrogen assisted intergranular cracking and blistering (26,28).

The precipitation process and associated hardening of 2024 aluminum occurs through the formation of three distinct transition structures and the development of the final equilibrium phase of the Cu-Al system. The transition structures formed are Gunier-Preston zones, GP-1 and GP-2, and θ' structure. These transition structures are precursors to the equilibrium structure $CuAl_2$ which is coherent with the aluminum matrix. Formation of the equilibrium

structure results in the attainment of the peak aged condition and has lattice dilations or strains associated with the precipitate. As the aging process continues, the lattice strains of the coherent precipitates reach a critical value and dislocation loops begin to form around the precipitate. The formation of dislocation loops destroys the precipitates coherency with the matrix and causes local softening or overaging. The aging process thus depends on microscopic lattice strain and dislocation formation. The interaction of strain fields with absorbed hydrogen could therefore effect the aging process because hydrogen is known to segregate to areas of high lattice dilation and effect interfacial strengths.

To determine what role, if any, hydrogen was playing in the precipitation process of 2024 aluminum, cubes of 2024 aluminum one inch on edge were cut from samples in the peak aged condition and were overaged in both dry air and hydrogen-water vapor environments at 240^{o}C (Figure 29). It was observed that samples tested in a hydrogen-water vapor environment overaged much more rapidly than those tested in a dry air environment for a given aging time. To elucidate the role of hydrogen in the aging process, the entire aging curve at 180^{o}C was constructed for both test environments (Figure 30). The aging kinetics for both environments is almost identical up to the peak hardness

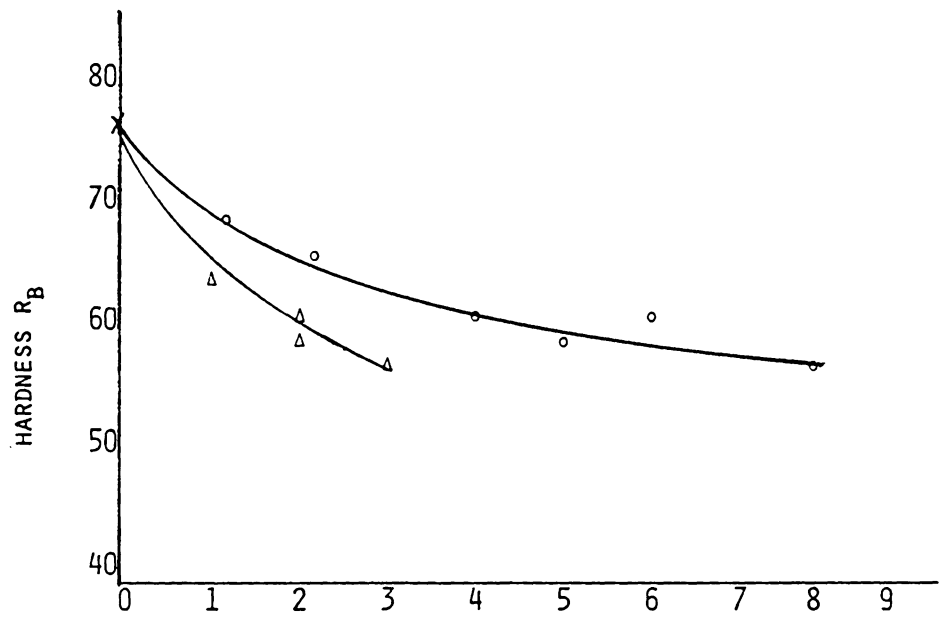

Figure 29

EFFECT OF TIME OF ANNEAL AT 240°C
ON THE HARDNESS OF 2024 ALUMINUM

o - AIR ENVIRONMENT

Δ - HYDROGEN-WATER VAPOR ENVIRONMENT

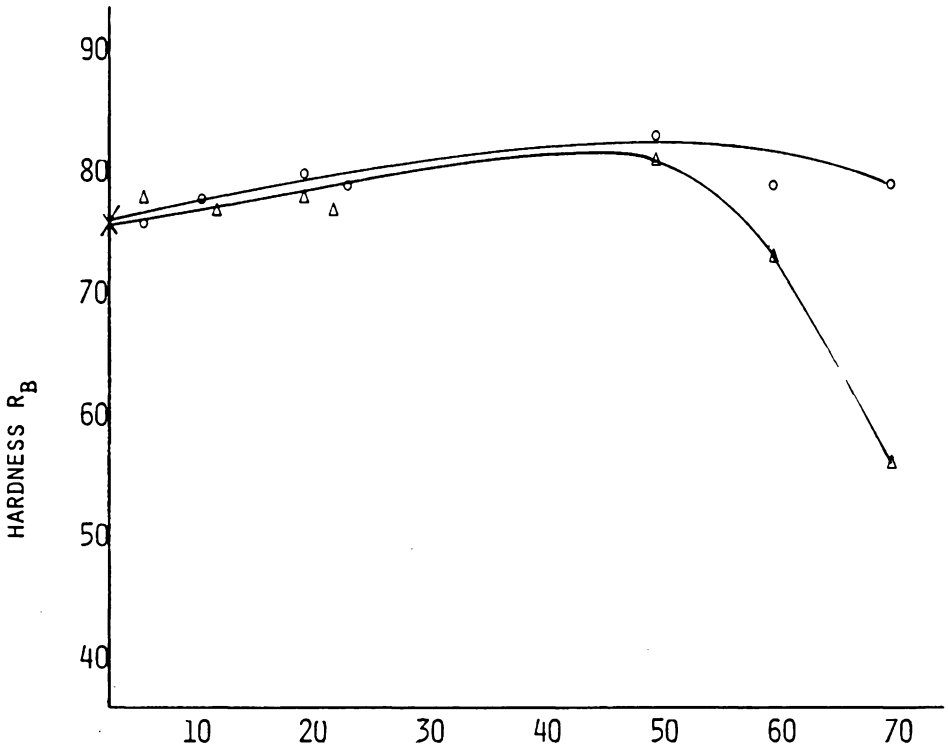

Figure 30

EFFECT OF TIME OF ANNEAL AT 180°C ON HARDNESS OF 2024 ALUMINUM

o - AIR ENVIRONMENT

Δ - HYDROGEN-WATER VAPOR ENVIRONMENT

value. However, as was observed in overaging tests at 240°C, samples tested in a hydrogen-water vapor environment overaged much faster.

The lack of observed environmental effects on the initial stages of aging (Figure 30) is probably due to the fact that no new interfaces have been created. The environmentally assisted rapid overaging is initiated by the absorption of high fugacity hydrogen generated from the high pressure hydrogen environment and the continuous reaction represented by Equation 1.

$$2Al + 3H_2O \rightarrow Al_2O_3 + 6H \qquad (1)$$

The absorbed hydrogen segregates to areas of high lattice dilations at the coherent θ-κ boundaries and is consistent with other investigators who noted that such segregation is maximized when lattice dilations are high (9). Thus, local regions of high hydrogen concentrations develop as aging proceeds. In this hydrogen rich interfacial region, local softening occurs by a premature loss of coherency due to an increased ease of dislocation nucleation (or interface formation).

For hydrogen to increase the ease of dislocation nucleation and therefore promote overaging, it must lower the energy of the system represented by Equation 2.

$$U_T = -U_c + U_\perp + U_H \tag{2}$$

where

U_T = energy associated with a loss of coherency.

U_c = energy associated with coherency strains.

$U_\perp$ = energy needed to form a dislocation in the absence of hydrogen.

U_H = energy associated with hydrogen.

With hydrogen absent from the system:

$$U_T = -U_c + U_\perp \tag{3}$$

For a loss of coherency to occur:

$$|U_\perp| < |-U_c| \tag{4}$$

However, in the present study, hydrogen has been charged into the samples and for a loss of coherency to occur Equation 4 becomes:

$$|U_\perp + U_H| < |-U_c| \tag{5}$$

It has been demonstrated that hydrogen binds to dislocations in 5086 aluminum (12). For this to be true:

$$|U_{\perp H}| < |U_\perp + U_H| \tag{6}$$

where $U_{\perp H}$ represents the total energy associated with hydrogen bonded to a dislocation. Substituting the left-hand side of Equation 6 into Equation 3, the energy necessary for over-aging in a hydrogen charged system becomes:

$$U_T = -U_c + U_{\perp H} \tag{7}$$

For hydrogen enhanced loss of coherency then

$$U_{\perp H} < U_{\perp} \tag{8}$$

and this condition is assumed to exist because of the binding observed in 5086 Al. To date, no study to confirm this trapping in 2024 Al has been conducted. However, it has been shown, indirectly, that by introducing hydrogen to aluminum, the shear modulus, G, is lowered (44).

$$U_{\perp} \alpha \tfrac{1}{2} Gb^2 \tag{9}$$

Since the lowering of G would lower $U_{\perp}$ so that $U_{\perp H} < U_{\perp}$, Equation 8 may well be valid. Therefore, assuming that hydrogen increases the ease of dislocation nucleation, the introduction of hydrogen to the system makes it easier to "punch-out" dislocations at the coherent θ precipitates and overaging occurs more rapidly.

Such a mechanism to account for hydrogen effects on the aging of aluminum can be used to explain hydrogen enhanced fatigue crack growth in peak aged aluminum. In fatigue testing, fatigue cycles expose new aluminum surfaces to the moist environment. These new surfaces are attacked by the moisture, thus the generation of hydrogen according to Equation 1 continually occurs. This hydrogen is absorbed at the high stress region of the crack tip, segregates to regions of high lattice dilations at the coherent θ' precipitates and promotes local softening.

This softening enhances fatigue crack growth and causes early failure.

This study, as did the studies with mild and stainless steels, indicates that hydrogen effects on the mechanical properties of metals and alloys are frequently associated with hydrogen segregation to interfaces. This segregation changes the interfacial characteristics and can readily promote premature fracture.

Section V

Conclusions

In this study of hydrogen effects on austenitic stainless steel, mild steel and aluminum, hydrogen redistribution during testing and hydrogen segregation to pre-existing sites prior to testing were shown to degrade mechanical properties. The hydrogen embrittlement processes in these materials occurred primarily by hydrogen induced weakening of various interfaces. In impact and slow bend tests of 21-6-9 and 304L stainless steels, the major hydrogen effect was to promote a faceted fracture along various interfaces in the metal lattice. The observation of hydrogen induced faceted fracture in impact tested samples at -197^{o}C indicates that hydrogen segregation during the test is not necessary to cause such embrittlement. However, the observation of enhanced embrittlement in samples tested in the slow bend mode demonstrates that hydrogen redistribution contributes to the overall hydrogen embrittlement process. Disk rupture tests on mild steel support the observation of hydrogen induced weakening of interfaces. Fractographic studies of hydrogen tested 1018 steel samples showed that the inclusion-matrix interfaces served as failure initiation sites. In addition, the discontinuous nature of crack growth in hydrogen tested samples indicates that a critical hydrogen concentration must develop at an interface before rapid

fracture takes place. Hydrogen effects on the age hardening characteristics of aluminum also indicate the importance of hydrogen segregation to interfaces. In the 2024 aluminum, hydrogen segregates to areas of high lattice dilation at the precipitate-matrix interface and high hydrogen concentrations develop. In this hydrogen charged region, a premature loss of coherency occurs due to an increased ease of dislocation nucleation.

All the above results are consistent with a decohesion type embrittlement mechanism, which holds that dissolved hydrogen reduces the cohesive strength of the lattice (9). Although these results support a decohesion mechanism of hydrogen embrittlement, such embrittlement takes place preferentially at interfaces and little or no evidence for hydrogen induced weakening of non-interfacial regions was obtained.

References

1. H. W. Kirkby and J. I. Morely, J. Iron Steel Inst., Vol. 158, p. 289 (1948).

2. J. P. Hirth, Script Metallurgica, Vol. 11B, p. 861 (1980).

3. L. Christodoulou, M. F. Stevens, J. J. Lewandowski, I. M. Bernstein, and A. W. Thompson, Environmental Degradation of Engineering Materials in Hydrogen, edited by M. R. Louthan, Jr., R. P. McNitt and R. D. Sisson, Jr., p. 161, Virginia Polytechnic Institute, Blacksburg, VA (1981).

4. M. R. Louthan, Jr., Hydrogen in Metals, edited by I. M. Bernstein and A. W. Thompson, p. 53, The Metallurgical Society of AIME, N.Y. (1981).

5. M. R. Louthan, Jr., G. R. Caskey, Jr., J. A. Donovan and D. E. Rawl, Jr., Materials Science and Engineering, Vol. 10, p. 289 (1972).

6. M. R. Louthan, Jr., R. D. Sisson, Jr., R. P. McNitt, and P. E. Smith, p. 829, ibid. Ref. 4.

7. G. G. Hancock and H. H. Johnson, Trans. AIME, Vol. 236, p. 513 (1966).

8. M. R. Louthan, Jr., and R. P. McNitt, Effect of Hydrogen on Behavior of Materials, edited by A. W. Thompson and I. M. Bernstein, p. 496, The Metallurgical Society of AIME, N.Y. (1976).

9. A. R. Troiano, Trans. ASM, Vol. 52, p. 54 (1960).

10. C. D. Beachem, Met. Trans., Vol. 3, p. 437, (1972).

11. P. Bastien and P. Azou, Proc. First World Metallurgical Congress, ASM, Cleveland, (1951).

12. M. R. Louthan, Jr., G. R. Caskey, Jr., J. A. Donovan and D. E. Rawl, Jr., Hydrogen Damage edited by C. D. Beachem, p. 289, ASM, Metals Park, OH (1977).

13. M. R. Louthan, Jr., D. E. Rawl, J. A. Donovan, and W. G. Holmes, "Hydrogen Embrittlement of Austenitic Stainless Steels", presented at The American Nuclear Society Annual Meeting, June 8-13, 1975, New Orleans, LA.

14. J. A. Donovan, "Release of Hydrogen from Metals During Plastic Deformation", presented at the AIME Fifth Annual Spring Meeting, May 29 - June 1, 1979, Philadelphia.

15. J. M. Hyzak, D. E. Rawl, Jr., and M. R. Louthan, Jr., Scripta Met., Vol. 15, p. 937 (1981).

16. G. R. Caskey, "Fractography of Hydrogen-Embrittled Stainless Steel", presented at the 106th AIME Annual Meeting, March 6-10, 1977, Atlanta, GA.

17. M. R. Louthan, Jr., and G. R. Caskey, to be published.

18. T. S. Sudarshan, M. R. Louthan, Jr., and R. P. McNitt, Scripta Met., Vol. 12, p. 799 (1978).

19. R. Garber, I. M. Bernstein and A. W. Thompson, Scripta Met., Vol. 10, p. 1210 (1976).

20. T. A. Adler, M. R. Louthan, Jr., and R. P. McNitt, Microstructural Science, edited by D. W. Stevens, G. F. VanderVoort and J. L. McCah, p. 217, The International Metallographic Society, N.Y. (1980).

21. J. Murali, T. A. Adler, T. S. Sudarshan, M. R. Louthan, Jr., and R. P. McNitt, Int. J. Hydrogen Energy, Vol. 5, p. 597, (1980).

22. J. P. Hirth, and O. A. Onyewuenyi, p. 133, ibid. Ref. 3.

23. P. W. Smith, M. R. Louthan, Jr., and R. P. McNitt, Scripta Met., Vol. 14, p. 199 (1980).

24. J. P. Fidelle, L. R. Allemand, C. Roux and M. Rapin, Hydrogen in Metals, p. 131, Valdic, France (1967).

25. J. P. Fidelle, R. Broudeur, C. Pirroriani and C. Roux, ASTM STP543 (1972).

26. M. O. Speidel, p. 249, ibid. Ref. 4.

27. W. L. Morris, M. R. James and R. V. Inman, Report NR 036-134. Rockwell International, Thousand Oaks, CA (1982).

28. J. Albrecht, I. M. Bernstein and A. W. Thompson, "Evidence of Dislocation Transport in Aluminum", to be published in Met. Trans.

29. D. A. Hardwick, M. Taheri, A. W. Thompson, and I. M. Bernstein, Met. Trans., Vol. 13A, p. 235 (1982).

30. A. J. West and M. R. Louthan, Jr., Met. Trans., Vol. 10A, p. 1675 (1979).

31. A. J. West, and J. H. Holbrook, Hydrogen Effects in Metals, edited by I. M. Bernstein and A. W. Thompson, p. 607, The Metallurgical Society of AIME, N.Y. (1980).

32. G. R. Caskey, Jr., Environmental Degradation of Engineering Materials, edited by M. R. Louthan, Jr., and R. P. McNitt, p. 437, Virginia Polytechnic Institute, Blacksburg, VA (1977).

33. I. M. Bernstein, R. Garber and G. M. Pressouyre, p. 37, ibid, Ref. 8.

34. R. C. Wasielewski, M. S. Thesis, Dept. of Materials Engineering, Virginia Tech (1982).

35. R. P. McNitt, R. D. Sisson, Jr., M. R. Louthan, Jr., B. A. Lewis, and J. A. Wagner, p. 785, ibid., Ref. 31.

36. R. D. Sisson, Jr., J. H. Wilson, T. A. Adler, R. P. McNitt and M. R. Louthan, Jr., Scripta Met., Vol. 14, p. 1207 (1980).

37. S. M. Milkovich, M. S. Thesis, Dept. of Materials Engineering, Virginia Tech (1981).

38. G. R. Caskey, "Acoustic Emission from Hydrogen", to be published in Scripta Met.

39. H. L. Dunegan and A. S. Tetelman, Engineering Fracture Mechanics, Vol. 2, p. 389 (1971).

40. C. A. Tatro, R. G. Liptal and D. W. Moon, Stress Corrosion Cracking and Hydrogen Embrittlement of Iron Base Alloys, edited by NACE, p. 509, NACE, Houston, (1977).

41. A. S. Tetelman, Met. Trans., Vol. 11, p. 13 (1971).

42. J. H. Wilson, M. S. Thesis, Dept. of Agricultural Engineering, Virginia Tech (1973).

43. J. Murali, M. R. Louthan, Jr. and R. P. McNitt, Optimization of Processing Properties and Service Through Microstructural Control, edited by H. Abrams, G. N. Maniar, D. A. Nail and H. D. Solomon, p. 382, ASTM, Philadelphia (1978).

44. J. C. Swearengen and F. A. Greulich, p. 303, ibid., Ref. 3.

The vita has been removed from the scanned document

Hydrogen Embrittlement: An Interfacial Phenomenon

by

John A. Wagner

(Abstract)

Hydrogen transport during a test and hydrogen segregation to twins, second phase particles and precipitation products prior to testing are shown to adversely effect the mechanical properties of metals. Hydrogen embrittlement processes in austenitic stainless steel, mild steel and aluminum occurred primarily by hydrogen induced weakening of the interfaces associated with specific metallographic features. In impact and slow bend tests of 21-6-9 and 304L stainless steels, the effect of hydrogen manifests itself in hydrogen induced faceted fracture along interfaces in the metal lattice. The extent of this weakening increases as the hydrogen content in the test sample is increased and during slow strain rate studies which promote hydrogen redistribution during the test. Disk rupture studies with 1015 and 1018 steels show that hydrogen segregation to the inclusion-matrix interface weakens the interface to such a degree that rapid fracture occurs. Studies with aluminum also indicate that hydrogen segregation to an interface degrades the mechanical properties. In age hardening experiments, hydrogen segregation caused an increase in the overaging kinetics in 2024 Al. This caused local

softening of the aluminum and was probably due to the effect of hydrogen in promoting a loss of coherency at precipitate-matrix interfaces. The combined results of these tests support a decohesion type embrittlement mechanism, with the decohesion occurring at the interfaces. The results also suggest that any decohesion type mechanism must take into account the importance of hydrogen segregation and dislocation transport of hydrogen in the embrittlement process.